

Utah State University

DigitalCommons@USU

All Graduate Theses and Dissertations

Graduate Studies

5-2014

Uncertainty Quantification of Photothermal Radiometry Measurements Using Monte Carlo Simulation and Experimental Repeatability

Austin Fleming
Utah State University

Follow this and additional works at: <https://digitalcommons.usu.edu/etd>



Part of the [Aerospace Engineering Commons](#)

Recommended Citation

Fleming, Austin, "Uncertainty Quantification of Photothermal Radiometry Measurements Using Monte Carlo Simulation and Experimental Repeatability" (2014). *All Graduate Theses and Dissertations*. 3299. <https://digitalcommons.usu.edu/etd/3299>

This Thesis is brought to you for free and open access by the Graduate Studies at DigitalCommons@USU. It has been accepted for inclusion in All Graduate Theses and Dissertations by an authorized administrator of DigitalCommons@USU. For more information, please contact digitalcommons@usu.edu.



UNCERTAINTY QUANTIFICATION OF PHOTOTHERMAL RADIOMETRY
MEASUREMENTS USING MONTE CARLO SIMULATION AND
EXPERIMENTAL REPEATABILITY

by

Austin Fleming

A thesis submitted in partial fulfillment
of the requirements for the degree

of

MASTER OF SCIENCE

in

Mechanical Engineering

Approved:

Dr. Heng Ban
Major Professor

Dr. Nick Roberts
Committee Member

Dr. Robert Spall
Committee Member

Dr. Mark R. McLellan
Vice President for Research and
Dean of the School of Graduate Studies

UTAH STATE UNIVERSITY
Logan, Utah

2014

Copyright © Austin Fleming 2014

All Rights Reserved

Abstract

Uncertainty Quantification of Photothermal Radiometry Measurements Using Monte Carlo Simulation and Experimental Repeatability

by

Austin Fleming, Master of Science

Utah State University, 2014

Major Professor: Dr. Heng Ban
Department: Mechanical and Aerospace Engineering

Accurate thermal property measurements are essential in the design process of any thermal system. Thermal wave techniques have been identified as a robust method to measure these types of samples; however, little uncertainty quantification has been provided. Photothermal Radiometry (PTR) is among the most common thermal-wave techniques for measuring thermal properties. PTR measurements are often conducted on two layer samples, where the top and bottom layers are referred to as the film and substrate, respectively. This work provides an understanding to the uncertainty associated with these types of two layer measurements through use of numerical and experimental techniques.

To perform this uncertainty quantification a Monte Carlo uncertainty simulation was performed. The simulation calculated statistical distributions for thermal diffusivity and effusivity for the top layer in a two-material sample. The simulation allows for input distributions for layer thicknesses, substrate thermal properties, frequency, and phase measurement. It has been determined PTR measurements can have accuracy on thermal conductivity in the 5% range and thermal diffusivity in the 10% range depending on the input distributions.

A numerical sensitivity study on the film thermal diffusivity and effusivity has been conducted for the input variables of film thickness, substrate diffusivity, substrate effusivity,

and frequency. The four non-dimensional parameters governing the two-layer thermal-wave heat transfer have been determined. From numerical results, experimental suggestions are provided to reduce uncertainty in measured values. These suggestions include: logarithmic spacing of frequency scan measurements, constraints on spot size and detection size, and the number of samples to take at each frequency.

A Photothermal Radiometry system has been designed, built, and calibrated. The system performed a frequency scan on a stainless steel 304 sample to verify heating spot size, detection spot size, and the transfer function used to remove the response of the system. A proton-irradiated zirconium carbide sample was measured by this PTR system in addition to two other international systems. This study provides insight to the good repeatability of PTR across systems and experimentalists.

(76 pages)

Public Abstract

Uncertainty Quantification of Photothermal Radiometry Measurements Using Monte Carlo Simulation and Experimental Repeatability

by

Austin Fleming, Master of Science

Utah State University, 2014

Major Professor: Dr. Heng Ban
Department: Mechanical and Aerospace Engineering

Photothermal Radiometry is a common thermal property measurement technique which is used to measure the properties of layered materials. Photothermal Radiometry uses a modulated laser to heat a sample, in which the thermal response can be used to determine the thermal properties of layers in the sample. The motivation for this work is to provide a better understanding of the accuracy and the repeatability of the Photothermal Radiometry measurement technique. Through this work the sensitivity of results to input uncertainties will be determined. Additionally, using numerical simulations the overall uncertainty on a theoretical measurement will be determined.

The repeatability of Photothermal Radiometry measurements is tested with the use of a proton irradiated zirconium carbide sample. Due to the proton irradiation this sample contains two layers with a thermal resistance between the layers. This sample has been independently measured by three different researchers, in three different countries and the results are compared to determine the repeatability of Photothermal Radiometry measurements. Finally, from sensitivity and uncertainty analysis experimental procedures and suggestions are provided to reduce the uncertainty in experimentally measured results.

Contents

	Page
Abstract	iii
Public Abstract	v
List of Tables	viii
List of Figures	ix
Acronyms	xi
1 Introduction	1
2 Literature Review	2
2.1 Overview of Photothermal Methods	2
2.1.1 Heating Strategies	2
2.1.2 MOR	3
2.1.3 Photoacoustic Detection	4
2.1.4 Photothermal Radiometry	4
2.1.5 Optical Beam Deflection (Mirage)	6
2.2 Thermal Wave Field Equations and Solutions	6
2.2.1 Thermal Wave Field Equation	8
2.2.2 Heating Regimes & One Dimsional Solution	9
2.2.3 Two Dimensional Axi-symmetric Solution	11
2.3 Detection Methods	12
2.4 PTR Instrumentation & Transfer Function	13
2.4.1 Laser Modulation	14
2.4.2 Detector	15
2.4.3 Transfer Function Methods	16
2.5 Monte Carlo Method	16
3 Objectives	19
4 Approach	21
4.1 Photothermal Radiometry Design	21
4.1.1 Laser	21
4.1.2 Laser Modulator	21
4.1.3 Infrared Radiation Sensor	22
4.1.4 Lock-In Amplifier	22
4.1.5 Radiation Collection Optics	22
4.1.6 Capabilities of System	22
4.2 Calibration of PTR System	23

4.3	Uncertainty Analysis	23
4.4	Measuring Thermal Properties	23
5	Experimental Setup	24
5.1	Laser	24
5.2	Modulator	25
5.3	Detector	26
5.4	Collection Optics	26
5.5	Lock-In Amplifier	29
5.6	Optic Accessories	30
6	Analytical and Numerical Results	32
6.1	Two Dimensional vs One Dimensional Heat Transfer	32
6.2	Non-Dimensional Analysis	34
6.3	Sensitivity	35
6.4	Log vs Linear Spacing	37
6.5	Monte Carlo Overall Uncertainty	38
7	Experimental Methods	43
7.1	Laser Modulation	43
7.1.1	Laser	43
7.1.2	Acousto Optical Modulator	44
7.1.3	Wave Form Generator	44
7.2	Mirror Alignment	45
7.2.1	1st Mirror and Sample	45
7.2.2	2nd Mirror and Detector	51
7.2.3	Changing Samples	52
7.3	Calibrating	52
7.3.1	Transfer Function	53
7.3.2	Calibration Sample	53
7.4	Taking Data	54
7.4.1	Specifying Scan	54
7.4.2	Lock-in Settings	55
8	Measured Results	56
8.1	Transfer Function Analysis	56
8.2	Stainless Steel	57
8.3	ZrC Irradiated Sample	59
9	Conclusions and Summary	61
	References	63

List of Tables

Table		Page
6.1	Correlations between input parameters and the fitted film diffusivity and effusivity	36
6.2	Table of the Monte Carlo input parameters and their uncertainty.	38

List of Figures

Figure	Page
2.1 Diagram of a Modulated Optical Reflectance system.	5
2.2 Diagram of a Photoacoustic system.	5
2.3 Diagram of a Photothermal radiometry system.	7
2.4 Diagram of a Optical Beam Deflection (mirage) system.	7
2.5 Diagram of thermal waves being induced into a two layer sample from a periodic heating.	10
2.6 Diagram of several heating conditions possible in PTR measurements. Heating scenario a: large spot size with a low modulation frequency; b: large spot with high modulation frequency; c: small spot size low modulation frequency.	11
2.7 Diagram of a Back Detection PTR system	14
2.8 Diagram of a general Monte Carlo Simulation Technique	18
5.1 Image of the 575mW ND:YAG, frequency doubled (532 nm) laser used in the PTR system.	26
5.2 Image of the Acousto Optical Modulator used in the PTR system.	27
5.3 Image of the Kolmar Technologies Mercury Cadmium Telluride infrared radiation detector used in PTR system.	28
5.4 Gold coated, off-axis parabolic mirror used in PTR system to increase the signal to noise ratio of the detector by collecting more IR radiation.	29
5.5 Image of the lock-in amplifiers used in the PTR system to filter out noise and amplify the detector signal at the modulation frequency.	30
6.1 Plot of: the phase of the surface temperature as a function of radius, the $\int_0^r \text{Amp}(r)\text{Phase}(r)dr$, the one dimensional phase, and the amplitude(r). The plot is given for a homogeneous sample of stainless steel with a heating spot radius of 20 μm	33

6.2	Integrated phase of the surface temperature as a function of radius plotted with the one-dimensional phase at the surface of a homogeneous sample. Plot is given for a homogeneous sample of stainless steel with a heating spot radius of 20 μm	33
6.3	Sensitivity plot of diffusivity and effusivity as the “measured” value for layer thickness is varied in the curve fitting process.	37
6.4	Comparison of logarithmic and linear frequency spacing. Bias uncertainty in effusivity and diffusivity are plotted as a function of the number of frequencies sampled.	39
6.5	Comparison of logarithmic and linear frequency spacing. Precision uncertainty in effusivity and diffusivity are plotted as a function of the number of frequencies sampled.	40
6.6	Diagram of the Monte Carlo Simulation applied to PTR.	42
7.1	Mirror misalignment in the z-direction.	46
7.2	The misalignment and the imaged formed if the laser is to the left of the focal point of the mirror. The target has been placed at the focal point of the mirror.	48
7.3	The misalignment and the imaged formed if the laser is to the right of the focal point of the mirror. The target has been placed at the focal point of the mirror.	48
7.4	The misalignment and the imaged formed if the laser is below the focal point of the mirror. The target has been placed at the focal point of the mirror.	50
7.5	The misalignment and the imaged formed if the laser is above the focal point of the mirror. The target has been placed at the focal point of the mirror.	50
7.6	The well aligned and corresponding image formed.	51
8.1	Plot of the transfer function obtained for the PTR system by detecting the laser light directly in the MCT detector.	58
8.2	Measured phase and predicted phase of a homogeneous stainless steel 304 sample with detection spot size of 0.5 mm and heating spot size of 0.5 mm.	58
8.3	Frequency scan of Proton Irradiated zirconium carbide sample. Plotted along side Horne and Jensen’s measurements of the same sample with different PTR systems.	60

Acronyms

AOM	Acousto Optical Modulator
DRP	Data Reduction Process
DRA	Data Reduction Algorithm
EOM	Electical Optical Modulator
FOV	Field of View
MCM	Monte Carlo Method
MCT	Mercury Cadnium Telluride
MOR	Modulated Optical Reflectance
ND	Neutral Density
PA	Photo Accoustic
PTR	Photothermal Radiometry
SNR	Signal to Noise Ratio
TEM	Transverse Electric Mode

Chapter 1

Introduction

Accurate thermal properties are critical in engineering problems for stress, thermal, and life predictions. Thermal property measurement techniques often require a specific geometry of a homogeneous material. However, in practice many materials are inhomogeneous, e.g. layered or composite materials, and need to be measured non-destructively. Additionally, non-standard sample geometries often need to be measured which results in the need for flexible measurement techniques. This is often where photothermal measurement techniques are applied. Photothermal measurement techniques, in general, are when a sample is heated by light and the thermal properties of the sample are determined from its response.

Photothermal Radiometry (PTR) is a common method among the photothermal techniques. Few researchers have provided uncertainty on PTR results in the past, and even fewer have provided adequate explanation of how these values were obtained. When conducting an experiment it is important to estimate and report the uncertainty of the results; it is also necessary to report what method was used to make this estimation. Since a thorough uncertainty and repeatability analysis of PTR has not been conducted, one of the objectives of this work is to provide a general uncertainty analysis for frequency domain photothermal radiometry measurements and provide guidelines for experimental design and data extraction based on those results.

To accomplish these goals a PTR system will need to be designed, built, and calibrated. Measurements on known samples will need to be conducted for comparison. Extensive numerical analysis will be needed to quantify the uncertainty in PTR measurements, which will be evaluated using the Monte Carlo Method. In addition, the repeatability of PTR experimental measurements will be investigated across PTR systems and experimentalists.

Chapter 2

Literature Review

This literature review begins with an overview of photothermal theory and measurement techniques. Next, the analytic solutions used to solve for thermal properties will be discussed along with the various heating regimes. Finally PTR will be discussed in more detail including the experimental aspects, and an overview of the Monte Carlo Uncertainty method will be given.

2.1 Overview of Photothermal Methods

Photothermal techniques are measurements that are based on the energy conversion of incident light into heat. With this broad definition, many measurement techniques fit into this category. However, this broad category can be organized by two different experimental parameters, the type of heating, and the type of detection strategy.

2.1.1 Heating Strategies

Heating strategies can be split into two main categories:

- Frequency Domain: Periodic heating
- Time Domain: Typically a pulse of heating

Time domain measurements typically utilize a quick pulse or flash of light, and observe the rapid heating and decay of temperature after the pulse. Laser flash is a very popular example of a time domain photothermal measurement that has been used to measure thermal diffusivity [1–3]. In laser flash the thermal response from the laser pulse is observed from the opposite side of the sample. The time it takes for the pulse of energy to travel through the sample can be used to determine the thermal diffusivity. Additionally there are other

measurement techniques that observe the temperature decay on the same side of the sample. Some of these theoretical models used include the response of layered materials [4, 5].

The frequency domain techniques periodically heat the sample and measure the amplitude and phase of the periodic temperature. Photothermal Radiometry, Modulated Optical Reflectance, and Photodeflection are some common frequency domain techniques that will be discussed in more detail in this chapter. Periodic heating has several benefits in layered samples where more detailed information about the sample can be attained. The periodic heating in photothermal techniques is typically attained by modulating a laser beam which allows for controlled heating of a precise location on a sample.

In addition to different heating techniques, photothermal measurements also differ in detection methods. The method of detection varies both in location and means of detecting the signal. There have been many heating and detection techniques used to measure thermal properties [6–10]. Some of the main detection techniques will be discussed in the following subsections.

2.1.2 MOR

Modulated optical reflectance (MOR) uses two laser beams of different wavelength to periodically heat the sample and detect the surface temperature. Similar to other photothermal, methods the heating laser beam is periodically modulated. The second laser, probe laser, is a low power continuous laser contacting the sample concentric with the heating laser, see Figure 2.1. The reflection of the probe laser will then be modulated due to the change in optical reflectivity as a function of temperature. A photodiode can then be used to sense the modulation of the reflected probe beam [11–14].

The signal from the reflected probe beam then contains information about the amplitude and phase of the sample's temperature which can be used to extract thermal properties of the sample. The probe laser is typically much smaller in diameter than the pump laser so it can detect a precise location on the sample. In MOR it is necessary to use two lasers of sufficiently different wavelengths such that the pump can be filtered out with either a short pass, long pass, or band pass optical filter. Therefore only the probe laser will be detected

by the photodiode. Both measurement techniques where the probe laser is concentric or off-set from the pump have proven to be useful for thermal property measurements [15]. MOR is limited to the use on reflective samples with a polished surface finish. This limitation is imposed since the MOR signal is dependent on the specular reflection of the probe laser beam.

2.1.3 Photoacoustic Detection

Alexander Graham Bell first discovered the Photo Acoustic (PA) effect in 1880 [11,16] and the PA method was one of the first photothermal methods developed. The Photoacoustic method relies on the samples interaction with surrounding air to detect the samples temperature modulation. Due to the periodic heating of the sample, the gas in contact with the sample also become periodically heated. This periodic heating causes a periodic thermal expansion and contraction of the air near the surface creating an acoustic signal. The Photoacoustic (PA) method uses microphones to detect these acoustic waves, see Figure 2.2. From this acoustic signal information about the samples thermal response to heating can be determined, and from that thermal properties can be determined.

2.1.4 Photothermal Radiometry

Photothermal Radiometry (PTR), originally developed by Nordal and Kanstad [17], is a non-contact and non-destructive method for determining a sample's thermal properties. PTR uses an intensity modulated light source to induce a periodic thermal response in a sample. In PTR the amount of IR radiation emitted is used to determine the modulation of the temperature of the samples surface. The amount of infrared (IR) radiation emitted from an object is proportional to the objects temperature to the fourth according to the Stefan-Boltzmann Law [18] given in Equation 2.1. This radiation is detected using a IR detector, most commonly a mercury cadmium telluride detector cooled by liquid nitrogen. An object emits infrared radiation in all directions, in an effort to collect more of this radiation, off-axis parabolic mirrors are used. This increases the signal to noise ratio of the experiment and can be used to control the detection area, see Figure 2.3. Photothermal Radiometry

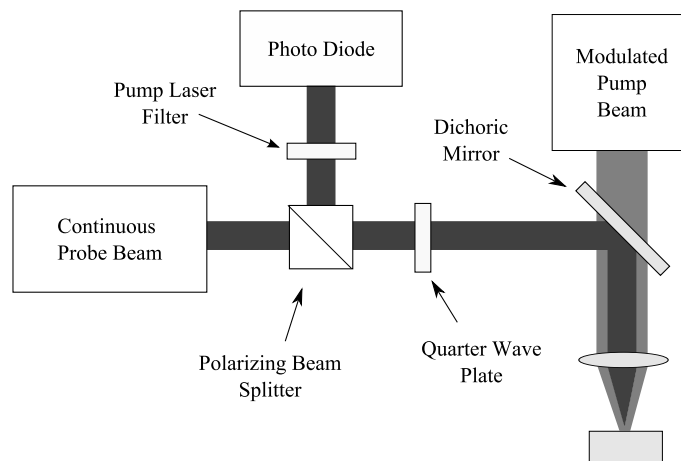


Fig. 2.1: Diagram of a Modulated Optical Reflectance system.

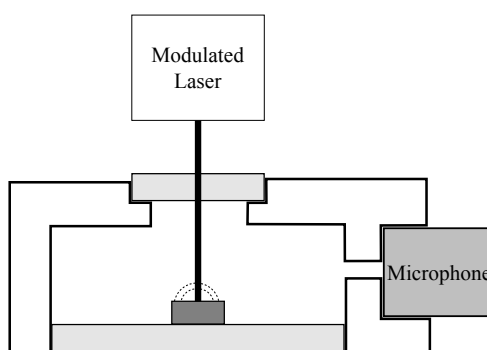


Fig. 2.2: Diagram of a Photoacoustic system.

has been proven as a reliable method to measure thermal properties, specifically those of layered materials [19–21]

$$E = \epsilon\sigma T^4 \quad (2.1)$$

2.1.5 Optical Beam Deflection (Mirage)

The Photothermal Deflection Technique, similar to the PA technique, detects the surface temperature through how it affects the surrounding air. The deflection technique uses a pump laser to periodically heat the sample with a probe laser traveling parallel to the surface of the sample, see Figure 2.2. The temperature changes of the surrounding air causes a change in the index of refraction of the air near the sample. As the probe laser travels through this area of heated air its direction is altered as it refracts through the change of index of refraction. Therefore, information about the samples temperature is contained in the change of direction of the probe laser. This change in direction can then be detected by a photodetector. This signal can then be used to calculate the thermal properties of the sample [22, 23].

2.2 Thermal Wave Field Equations and Solutions

Frequency domain photothermal methods use a periodically modulated laser to induce thermal waves into the sample and collect information about the modulating temperature of the sample to collect information about the sample. If the sample is layered, the induced thermal waves will be partially reflected and transmitted at material interfaces in the sample [11, 24]. These reflections and transmissions will cause temperature interference effects on the surface of the sample. The interference will affect both the amplitude and the phase of the thermal wave. While these interferences may be small, they are detectable, and can yield important information about the sample being measured.

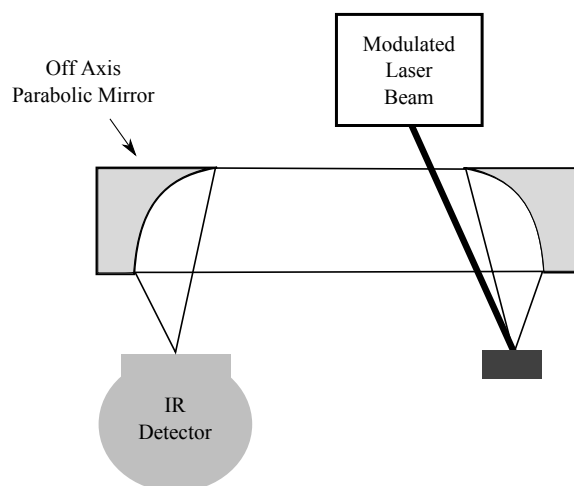


Fig. 2.3: Diagram of a Photothermal radiometry system.

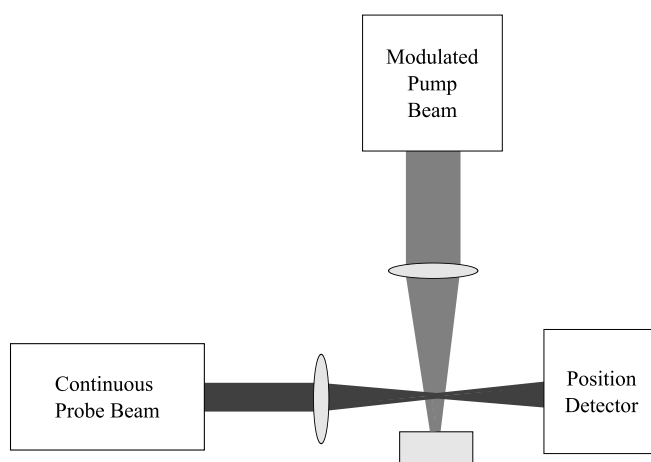


Fig. 2.4: Diagram of an Optical Beam Deflection (mirage) system.

This section will discuss the derivation and application of the thermal wave field equations, different modulated heating regimes that exist, and a few solutions to specific heating regimes including the interference effects from layered materials.

2.2.1 Thermal Wave Field Equation

The objective in thermal frequency domain photothermal techniques is to periodically heat the surface of a sample, and measure the periodic temperature response of the sample. Since the temperature response is periodic it is measured in means of amplitude and phase relative to the heating laser. Additionally, the temperature measurement is conducted in a frequency domain making it is useful to transform the heat equation into the frequency domain by use of Fourier transforms. This transformed heat equation will be referred to as the thermal wave field equation. This derivation is conducted by Mandelis [25], but will also included here because of its significance to the frequency domain photothermal methods.

Beginning with the heat conduction equation

$$\nabla^2 T(\mathbf{r}, t) - \frac{1}{\alpha} \frac{\partial T(\mathbf{r}, t)}{\partial t} = -\frac{1}{k} q(\mathbf{r}, t) \quad (2.2)$$

where α is the thermal diffusivity, k is the thermal conductivity, \mathbf{r} is the three dimensional position, and q is the volumetric heat generation. With the Fourier Transform of $T(r, t)$ defined as

$$\Theta(\mathbf{r}, \omega) = \int_{-\infty}^{\infty} T(\mathbf{r}, t) e^{-i\omega t} dt \quad (2.3)$$

equation 2.2 becomes

$$\nabla^2 \int_{-\infty}^{\infty} T(r, t) e^{-i\omega t} dt - \frac{1}{\alpha} \int_{-\infty}^{\infty} \left(\frac{\partial T(r, t)}{\partial t} \right) e^{-i\omega t} dt = -\frac{1}{k} \int_{-\infty}^{\infty} q(r, t) e^{-i\omega t} dt. \quad (2.4)$$

By defining

$$\sigma(\omega) = \sqrt{i\omega/\alpha} \quad (2.5)$$

where σ is called the complex wave number, equation 2.4 will become

$$\nabla^2\Theta(\mathbf{r},\omega) - \sigma^2\Theta(\mathbf{r},\omega) = -\frac{1}{k}q(\mathbf{r},\omega). \quad (2.6)$$

This is the equation that will be referred to as the thermal-wave-field equation. In equation 2.4, θ is the complex temperature where the magnitude and phase are given by the absolute value and the argument respectively.

The thermal-wave-field equation has been applied in many different ways. It has been used to measure thermal properties and thicknesses of layers in a sample [26]. It becomes very useful for the case where the sample contains layers of different material. Where the layer interfaces occur, the thermal waves will reflect and refract, similar to optical or acoustic waves [11]. It is easy to conceive how different number of layers and layers with different thermal properties will have very different solutions to the thermal-wave-field equation. These solutions methods include series solutions, quadrupole method, Greens functions, and optical methods. The two solutions that will be provided are for n-layer samples. Figure 2.5 shows a two layer sample with laser heating on the surface.

2.2.2 Heating Regimes & One Dimsional Solution

The frequency domain photothermal techniques rely on measuring the amplitude and phase at some location on the sample and relating that back to the samples properties. The characteristics of the heat transfer will vary depending on the heating spot size, the frequency of modulation, and material properties of the sample. This presents the need for various solutions depending on what heating regime and detection method is being used. The periodic heating induces thermal waves, very similar to acoustic waves except for they are very heavily attenuated. The thermal wave direction is dependent on the frequency of modulation, spot size, and thermal properties. The thermal diffusion length, μ defined in equation 2.7 where α is the samples thermal diffusivity and ω is the modulation frequency, is a critical parameter in determining the heating regime of the material.

$$\mu = \sqrt{\frac{2\alpha}{\omega}} \quad (2.7)$$

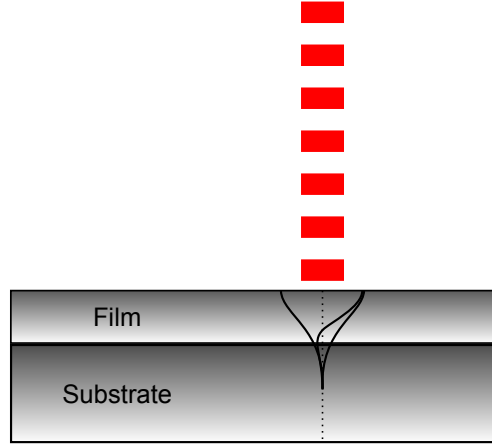


Fig. 2.5: Diagram of thermal waves being induced into a two layer sample from a periodic heating.

It has been determined by Almond and Patel [11] that if the heating spot size is >20 times the thermal diffusion length the heating regime follows a one dimensional solution where the surface is being uniformly heated, and thermal waves propagate normal to the surface. Figure 2.6 provides a visual depiction of how the spot size and thermal diffusion length effects the propagation of the thermal waves. This one dimensional solution for a layered material is given by Mandelis [25], and is presented here in Equations 2.8-2.12 where F_o is the laser flux, k is thermal conductivity, b is the ratio of thermal effusivities, h is the convection coefficient, i is the imaginary number, j is used to denote the layer, and N denotes the number of layers.

$$\Theta_1^{(N)}(\omega) = \frac{F_o}{4k_1\sigma_1} \left(\frac{(1 + R_1)[1 + \rho^{(N)}e^{2\sigma_1 L_1}]}{1 - R_1\rho_{21}^{(N)}e^{-2\sigma_1 L_1}} \right) \quad (2.8)$$

$$\rho_{j+1,j}^{(N)} = \frac{(1 - b_{j+1,j}) + \rho_{j+2,j+1}^{(N)}(1 + b_{j+1,j})e^{-2\sigma_{j+1}L_{j+1}}}{(1 + b_{j+1,j}) + \rho_{j+2,j+1}^{(N)}(1 - b_{j+1,j})e^{-2\sigma_{j+1}L_{j+1}}} \quad (2.9)$$

$$\rho_{N,N-1}^{(N)} = \frac{(1 - b_{N,N-1}) + R_N(1 + b_{N,N-1})e^{-\sigma_N L_N}}{(1 + b_{N,N-1}) + R_N(1 - b_{N,N-1})e^{-2\sigma_N L_N}} \quad (2.10)$$

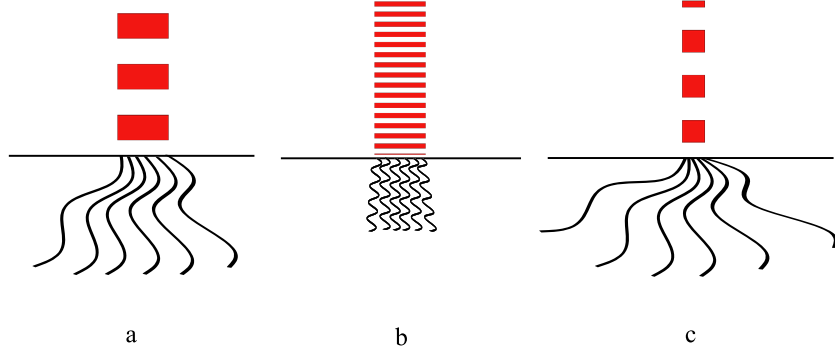


Fig. 2.6: Diagram of several heating conditions possible in PTR measurements. Heating scenario a: large spot size with a low modulation frequency; b: large spot with high modulation frequency; c: small spot size low modulation frequency.

$$R_j = \frac{k_j \sigma_j - h_j}{k_j \sigma_j + h_j} \quad (2.11)$$

$$\sigma_j = \sqrt{\frac{i\omega}{\alpha_j}} \quad (2.12)$$

2.2.3 Two Dimensional Axi-symmetric Solution

If the thermal diffusion length does not meet this one dimensional criteria then a heating state where the thermal waves propagate both into the sample and radially away from the laser spot. When the thermal diffusion length is much greater than the spot size, the thermal waves travel radially away from the laser spot in a hemisphere shape. In-between the two limiting cases the heating is axi-symmetric about the center of the heating spot. A solution for this axi-symmetric case due to a Gaussian heating profile is given by

Mandelis [25]:

$$\Theta(r, z, \omega) = \frac{F_0 W^2}{2k_1} \int_0^\infty \frac{(1 + R_1(\lambda))(e^{-s_1 z} + \rho_{21}^{(N)}(\lambda)e^{-s_1(2L_1 - z)})}{s_1(\lambda)(1 - R_1(\lambda)\rho_{21}^{(N)}(\lambda)e^{-2s_1 L_1}} e^{-(\lambda W/2)^2} J_0(\lambda r) \lambda d\lambda \quad (2.13)$$

$$\rho_{j+1,j}^{(N)} = \frac{(1 - \zeta_{j+1,j}) + \rho_{j+2,j}^{(N)}(1 + \zeta_{j+1,j})e^{-2s_{j+1}L_{j+1}}}{(1 + \zeta_{j+1,j}) + \rho_{j+2,j}^{(N)}(1 - \zeta_{j+1,j})e^{-2s_{j+1}L_{j+1}}} \quad (2.14)$$

$$\zeta_{i,j} = \frac{k_i \sqrt{\lambda^2 + \sigma_i^2}}{k_j \sqrt{\lambda^2 + \sigma_j^2}} \quad (2.15)$$

$$s_j(\lambda) = \sqrt{\lambda^2 + \sigma_j^2} \quad (2.16)$$

$$R_j(\lambda) = \frac{k_j S_j(\lambda) - h_j}{k_j S_j(\lambda) + h} \quad (2.17)$$

In Equations 2.13-2.17 F_0 is the laser flux, k is thermal conductivity, σ defined as in 2.5, W is the diameter of the laser beam, h is the convection coefficient, λ is a variable of integration, J_0 is the Bessel function, i is the imaginary number, j is used to denote the layer, and N denotes the number of layers. It is important to note in equations 2.13-2.17 the magnitude and phase are a function of r . Therefore the size, shape, and location of the detection will affect the amplitude and phase measured. It was shown by Almond and Patel that even with focused spots at high frequencies the solution will eventually limit to the one dimensional solution [11]. It has also been shown that if the detection integrates radially until the signal is diminishingly small, concentrically about the heating spot, the one dimension response is also obtained [27].

2.3 Detection Methods

This study is focused on the frequency domain Photothermal Radiometry method. However, even inside of frequency domain PTR there are other variations of the experimental technique. These remaining techniques can be split into front and back detection, which

the differences will briefly be discussed.

Front Detection

The front detection method observes the infrared radiation emitted by the sample from the same side as the laser is heating as displayed in Figure 2.3. This method is also known as the reflection method which is misleading because the infrared radiation detected is emitted from the surface not reflected. Therefore, in this paper it will only be referred to as the front detection method. The front detection method can be used on thick samples and typically has the highest signal to noise ratio because the temperature changes are the largest at the heating location. When using the modulated PTR method, front detection is typically utilized because the thermal waves created by the periodic heating are heavily attenuated as they pass through the sample. The amplitude of these waves are the largest at the surface, and if the sample is thick will be impossible to detect at the back surface.

Back Detection

In the back detection method, also known as the transmission method, the infrared detector observes the radiation emitted from the opposite side of the sample from the heating laser. In this method the thermal fluctuation induced at the surface travels through the sample is observed at the rear surface, see Figure 2.7. This method has a lower signal to noise ratio, and cannot be used on thermally thick samples. However the back detection method is not as effected by surface features as the front detection technique [9,28].

2.4 PTR Instrumentation & Transfer Function

As previously stated, PTR is different from other techniques in that it uses the infrared radiation emitted from the sample to detect the sample's temperature. This is beneficial because all materials emit infrared radiation allowing for a broad range of samples to be measured. However, it can be difficult to measure highly reflective materials because of the low absorptivity/emissivity. The low absorptivity will minimize the amplitude of the thermal waves. In addition the low emissivity will reduce the amount of radiation emitted

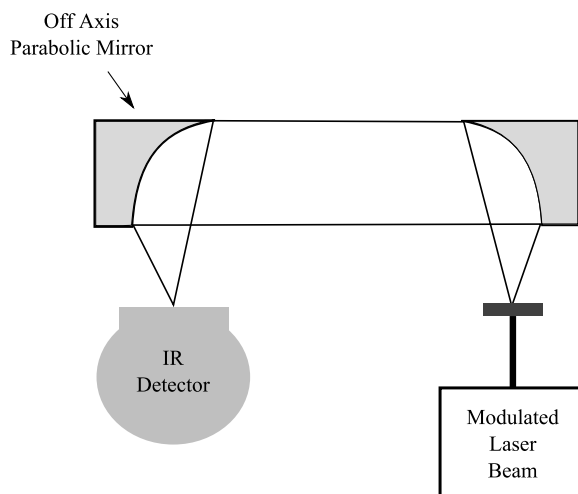


Fig. 2.7: Diagram of a Back Detection PTR system

by the sample reducing the signal obtained. Thus making extracting accurate phase and amplitude data challenging. This section will discuss the instrumentation and procedures necessary to detect the modulating temperature using a PTR system.

In a PTR experiment a modulated laser, collection optics, infrared detector, and lock-in amplifier are needed. Each of these components will be discussed briefly here.

2.4.1 Laser Modulation

Two common methods for generating a modulated laser include: Laser diode that can be modulated directly or a continuous Laser with an external modulator. A few examples of external modulators are an Acousto-Optical Modulator (AOM), Electro-Optical Modulator (EOM), or a Mechanical Chopper.

Electro-optical modulator

Electro-optical modulators(EOM) can be used to modulate the intensity of a laser. They are typically made of a lithium niobate crystal and utilize the Kerr effect to rotate the polarization of light as a function of the surrounding electric field [29]. By modulating the EOM's surrounding electric field the polarization of the light passing through it's crystal

will also be modulated. The intensity can then be modulated by passing this polarization modulating beam through a polarizing filter [30].

Acousto-optical modulator

Acousto-optical modulators (AOM) use the interaction between phonons and photons to modulate the intensity of the laser beam. The stationary waves of phonons cause variations in the density of the crystal. The light passing through the crystal then diffracts when it interacts with these density variations. By modulating the amplitude of the phonons in the crystal the diffraction will also be modulated. By utilizing the first order diffracted beam, full attenuation can be attained along with a high transmission efficiency at the lowest attenuation [29].

Mechanical Chopper

Another option that is often much cheaper than an EOM or AOM is a device that mechanically “chops” the laser. These are often spinning disks with slits cut in them to allow light through for a specific amount of time depending on how fast the disk is spinning and the size of the slit. Mechanical choppers are limited to a square wave form, where EOM’s and AOM’s can modulate pure sinusoidal waves.

2.4.2 Detector

PTR relies on being able to detect small changes in temperature by the change in emitted infrared radiation. To achieve this, very sensitive detectors with large amplification are needed. In addition, the detector needs to be sensitive at or around the peak emission wavelength, Weins wavelength, which is a function of the samples temperature [18, 31]. Weins wavelength is approximately $10\mu m$ at room temperature where most PTR systems are used. Mercury cadmium telluride (MCT) detectors have a peak sensitivity around $8-11\mu m$ which makes them common in PTR systems.

Even with the high sensitivity and amplification, often the useful PTR signal is smaller than the noise level. Therefore, requiring sophisticated electronics to pull out the useful

data. Typically a lock-in amplifier is used to filter all frequencies except around the frequency of the heating laser modulation. Once filtered and amplified, lock-in amplifiers can accurately measure the amplitude and phase of the signal.

2.4.3 Transfer Function Methods

In any experimental setup the equipment has limitations on the range of frequencies it can operate in. When periodic signals are processed by equipment both the amplitude and phase of the signal can be altered [32]. If the phenomena being measured is slow compared to the operating speed of the equipment this is often not a concern of experimentalists. However, if the speed of the equipment is comparable to the phenomena being observed then the lag from the equipment needs to be taken into account. Photothermal methods often require a very precise measurement of the phase and amplitude of a periodic signal, and often the excitation frequencies are several kHz where some equipment will noticeably alter the signal. This is the reason much care is taken in developing a method to remove the effect of the equipment. The values found to remove the effects of the equipment will be called the “Transfer Function” in this study. The Transfer Function is a set of phase lags and gain variation at a set of frequencies. Some researchers will take many data points and fit a curve to the Transfer Function, and use the fitted curve to account for the system response. After determining the values for the Transfer Function, it can be applied by subtracting out the phase lag and dividing the amplitude to obtain the data unaffected by the system. Experimentalists have proposed different methods to measure the system response. These methods include: observing the laser without the heating of a sample or using calibration samples such as stainless steel or vitreous carbon.

2.5 Monte Carlo Method

In any experiment it is critical to report how certain the results are. Two methods of propagating measurement uncertainties through a data reduction process are commonly used in practice: the Taylor’s series method and the Monte Carlo method (MCM). The first method is widely used primarily due to its theoretical and practical simplicity. The

second method, the Monte Carlo uncertainty propagation, has found increased use more recently as computers have become sufficiently powerful to handle the computational costs associated with it [33–35].

The MCM uses random input values into a simulation, and from these inputs determines the output, see Figure 2.8. The random input variables are based on probability distributions that are specific to the input variable. The parent distributions from where the input variables are generated can be determined from equipment specifications or measurements to determine the appropriate distribution. After many simulations are conducted the output distributions will converge and yield important information about the measurement uncertainty on the output based on the input uncertainties [36].

In determining the propagation of uncertainty in PTR measurements it is necessary to use the MCM because a fitting procedure is used to determine the output instead of solving an equation directly. The MCM is also advantageous because any distributions can be used for input variables, and is therefore not limited to Gaussian distributions similar to other techniques.

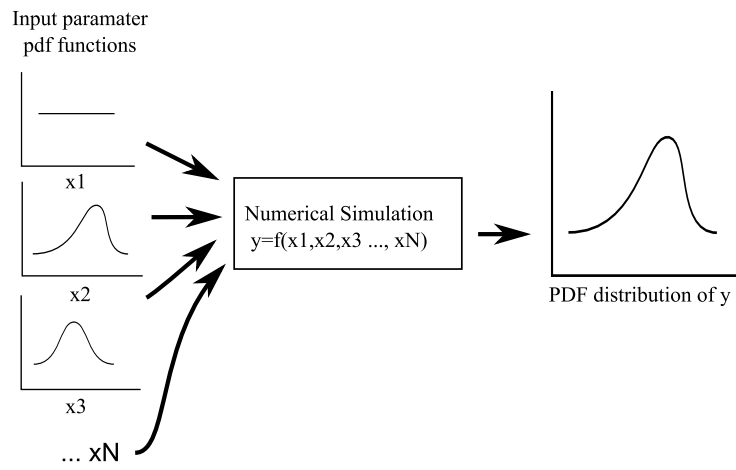


Fig. 2.8: Diagram of a general Monte Carlo Simulation Technique

Chapter 3

Objectives

The main objective of this work is to design, build, and calibrate a PTR system, and quantify its uncertainty. The system will be designed for room temperature, and have a capability to measure a wide variety of samples. Specifically the objectives will be:

1. Design, assemble, and calibrate a versatile PTR system.
2. Quantify general uncertainty in PTR measurements using Monte Carlo Uncertainty Analysis.
3. Determine the repeatability of PTR measurements by measuring a ion irradiated zirconium carbide sample.

The task list to accomplish the objectives follows:

1. Thermal wave background
 - (a) Conduct literature review on photothermal techniques and thermal wave background
2. Experimental Design and Setup
 - (a) Design a versatile PTR system
 - (b) Determine suitable experimental components for PTR system
 - (c) Assemble and Align system such that detection and heating spots are concentric and of well known size
3. Numerical and Analytical Results

- (a) Determine dimensionless constants of thermal wave problem
- (b) Determine input distributions for Monte Carlo Simulation
- (c) Calculate overall measurement uncertainty using Monte Carlo Simulation
- (d) Determine sensitivities of measured results to input variations

4. Experimental Testing

- (a) Measure system transfer function to remove the system's response in the measurement
- (b) Measure a Stainless Steel Calibration sample to verify accuracy of the measured system transfer function
- (c) Measure ion irradiated Zirconium Carbide sample

Chapter 4

Approach

This chapter will discuss the methods that will be applied in the design, calibration, and testing of the PTR system.

4.1 Photothermal Radiometry Design

The first task in designing a PTR system is to determine which testing procedure will be used experimentally. This will alter the specifications necessary for the equipment. In this work a front-detection, frequency-domain, system will be designed. For this technique, a light source, light modulator, infrared collection optics, infrared sensor, and lock-in amplifier are all necessary. Each component and its necessary specifications will now be discussed.

4.1.1 Laser

Lasers are the most common source of light used in the photothermal methods. Ease of modulation and power availability are the main reasons for this. There are three main types of lasers: diode, solid state, and gas. In selecting a laser the most important parameters to consider are power, power stability, wavelength of light, beam quality, divergence, polarization, and cost. In the design process each of parameters will be examined and an acceptable laser will be selected.

4.1.2 Laser Modulator

As discussed in Chapter 2, the four main methods to modulate a laser include: a mechanical chopper, acoustic optical modulator, electro optical modulator, and intracavity modulation. These methods will be compared on operational frequencies, wave form, quality of modulation, and cost. After these considerations an appropriate modulator for PTR measurements will be selected.

4.1.3 Infrared Radiation Sensor

The infrared radiation detector is a very important piece of equipment for a PTR experiment because it is the means by which the surface temperature is determined. There are many different types of infrared detectors and they all operate on slightly different principles. They have various detectivities, sensitivities, signal to noise ratios (SNR), and spectral response's. In the design process a detector will be selected that has an appropriate sensitivity for room temperature measurements, a sufficiently small rise time, and has the necessary sensitivity to capture the surface temperature oscillations.

4.1.4 Lock-In Amplifier

The modulated PTR experiments often exploit the phase vs frequency relationship that was developed from Photoacoustic techniques. Specialized hardware is necessary to capture this phase signal accurately as the frequency is varied. The typical piece of equipment used to measure this phase is a Lock-In Amplifier. The specifications necessary for a lock-in amplifier are: sensitivity, operating frequency range, phase resolution, and signal to noise capability.

4.1.5 Radiation Collection Optics

Infrared radiation is emitted in all direction from the samples surface. The infrared detectors are quite good at sensing this radiation, but to improve the signal to noise ratio optics are generally used. These optics also help decrease the area of the sample the detector is sensing. Therefore it can sense where the sample is being heated, and collect more of the infrared radiation being emitted from that same location. Both mirrors and lenses have been used in the design of PTR systems, but the important parameters are the same in both setups.

4.1.6 Capabilities of System

The design system will need to be capable of detecting the alternating component of samples temperature, and use that signal to determine the phase. It will need to be able to

operate on a large range of frequencies to accommodate different material properties and layer thicknesses. The system will also need to be sensitive to the 10 μm infrared radiation wavelength given off at room temperature.

4.2 Calibration of PTR System

In this work, a procedure to develop a suitable transfer function will be tested to determine which one is most appropriate and accurate. From literature allowing laser light to be directly measured by detector, and using calibration samples of vitreous carbon or stainless steel are the most common in practice.

4.3 Uncertainty Analysis

Monte Carlo uncertainty analysis will be performed to determine the overall uncertainty of a typical two layer photothermal radiometry measurement. This uncertainty analysis will be conducted as described by Coleman and Steele [36], who in turn follows directions set by the International Standard Organization (ISO). The uncertainty of the input parameters of the PTR process will be characterized. The input parameters to be characterized include layer thickness, thermal properties, and frequency. Thermal diffusivity and effusivity are typically the measured parameters in PTR. Therefore the sensitivities of these thermal properties will be calculated with respect to each of the input parameters. Additionally, the validity a 1-D heat transfer assumption will be investigated, along with a comparison between logarithmic and linear spacing of frequency data samples.

4.4 Measuring Thermal Properties

The properties of the zirconium carbide will be measured with the PTR system. The measurement will use the frequency scan method to determine the thermal properties of the sample. The results will be compared to those in literature [6, 37] to determine the reproducibility of PTR systems with different components and different operators.

Chapter 5

Experimental Setup

This chapter will discuss the PTR system design. The critical parameters of each component in a PTR system will be discussed, along with the reasoning for the decisions on each component.

5.1 Laser

The laser is critical in any photothermal method since it is what induces the thermal response in-which is being detected. It was determined early on, for ease of alignment and safety reasons it would be advantageous for the laser wavelength to be in the visible spectrum. In addition to this requirement, the heating power for PTR systems typically needs to be greater than 150 mW to induce a thermal wave capable of being detected.

The laser profile can play an important part in the heating of the sample. In two dimensional solutions such as the one given in the literature review, the heating source is assumed to be from a Gaussian laser beam. The laser profile is determined by what are called "transverse modes". They are determined by the laser cavity shape, and it's boundary conditions. In lasers with a cylindrical cavity the lowest order transverse mode is referred to as TEM00. This is denoting the transverse electric and magnetic modes are both at the lowest order. When this is the case the profile of the laser beam is a Gaussian. Another parameter of the shape of a laser beam is the m^2 factor. This factor compares the profile of a laser to that of an ideal Gaussian beam. A perfect Gaussian laser beam would yield a value of 1. While it is not necessary to use a Gaussian beam to conduct PTR measurements, in some cases the analytic solutions provided require a Gaussian beam when the one dimensional criteria is not met.

The beam diameter is also an important characteristic of the laser. Depending on what

the detection spot size will be, it can be advantageous to have either a much larger heating spot size or a much smaller heating spot size. To ensure the one dimensional heating as discussed in Chapter 2.

For this PTR system it was determined that a frequency doubled ND:YAG laser would fit the requirements of the system the best. The laser selected is shown in figure 5.1. The laser selected has a maximum power of 575 mW, transverse mode TEM00, linear polarization, beam diameter of 1mm. This is a diode-pumped solid-state laser. The laser cavity emits 1064 nm (Infrared) wavelength of light before it is frequency doubled. After it is frequency doubled the light has a 532 nm (green) wavelength, and any remaining infrared light is filtered out. ND:YAG's are efficient lasers, and are very common driving the cost of manufacturing down. Having the ability of outputting up to 575 mW also allows for numerous optics without concern of attenuating the laser to the point it will no longer induce a thermal wave large enough to be detected.

5.2 Modulator

In the design of this PTR system it was critical to maintain a wide range of operation to increase the variety of samples that can be measured. Often if a sample has a thin top layer, high modulation frequencies are needed for the thermal waves to interact with the interface between layers. With this high frequency limitation mechanical choppers and intra-cavity modulation were not feasible. The two options remaining are electro-optical modulators (EOM) and acousto-optical modulators (AOM). AOMs are limited to the carrier frequency of the AM modulation of the crystal. Theoretically EOMs have higher operating frequency because their modulation only relies on the modulation of an electric field around the lithium niobate crystal. However, EOMs require a high voltage to attain modulation and the crystals act as a capacitor. From electromagnetic theory, it is known that capacitors impedance reduces as a function of frequency. This causes the drivers for high frequency EOMs to be very high power and therefore very expensive.

For the design of this PTR system it was determined that an AOM would be appropriate. The AOM and driver were attained from Gooch and Housego, model number 35085-3.



Fig. 5.1: Image of the 575mW ND:YAG, frequency doubled (532 nm) laser used in the PTR system.

The AOM is made of fused silica with an acoustic aperture size of 3 mm. The AOM can be seen in figure 5.2.

5.3 Detector

Room temperature PTR systems most commonly use mercury cadmium telluride (MCT) detectors because their peak sensitivity is near $10 \mu m$, depending how they are doped. The physical size of the detector can also be a critical parameter in the decision of the detector. Typically larger detectors require a larger rise time making their maximum operating frequency lower. However, the smaller the detector, the smaller effective area which leads to a lower signal. This drives a compromise between operating speed and signal to noise ratio. The KLD-0.5-J1/11/DC from Kolmar Technologies is the detector used in this research which is shown in figure 5.3. This detector has a 0.5mm x 0.5mm chip size. This provides a large bandwidth with a cutoff frequency of 5MHz. This detector has a built in preamplifier which provides an overall response of 40,000 V/Watt between the response of the detector and the amplification. The full angle field of view is 60 degrees which allows for matching with an off-axis parabolic mirror which will be discussed next.

5.4 Collection Optics

The collection optics in PTR systems serve two main functions. They are to increase the

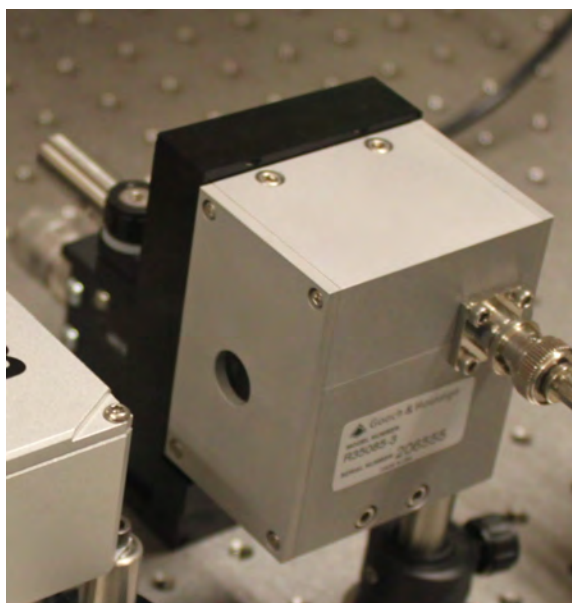


Fig. 5.2: Image of the Acousto Optical Modulator used in the PTR system.

signal from the detector by collecting more infrared radiation, and to adjust the detection area. The most common collection optics for PTR systems are off-axis parabolic mirrors. These mirrors have the capability to focus parallel beams of light into a focal point, and take rays emitted from a focal point and reflect them into a parallel beam. Therefore two off-axis parabolic mirrors are used. The focal point of the first mirror is positioned at the heating spot on the sample, and the focal point of the second mirror is located on the surface of the detector. This forms an image on the sample that the detector can "see" through the parabolic mirrors. The size of this image is determined by the size of the detector, and focal lengths of the mirrors. For a close approximation the size of the image on the sample is scaled by the ratio of the focal lengths of the mirrors. As previously discussed, it is important to know the detection spot size, particularly in comparison to the heating spot size. One of the off-axis parabolic mirrors used in this research can be seen in figure 5.4.

MCT detectors have a specified field of view (FOV) that is determined by a shield in the detector housing that is cooled by liquid nitrogen. Radiation that is coming in past the FOV angle will be blocked by this cold filter, and will not be sensed by the detector.



Fig. 5.3: Image of the Kolmar Technologies Mercury Cadmium Telluride infrared radiation detector used in PTR system.

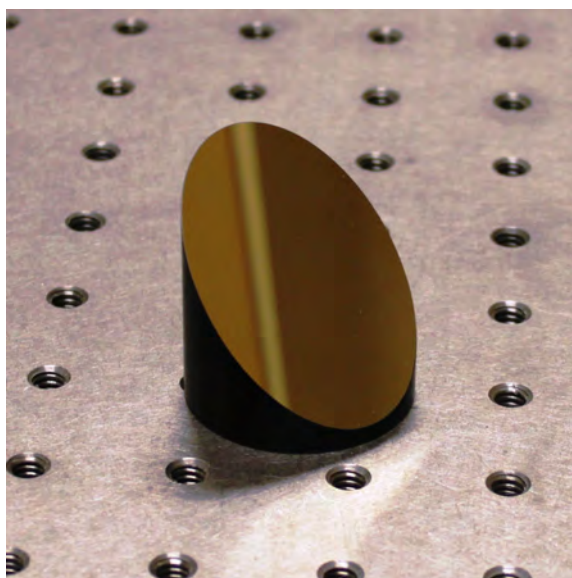


Fig. 5.4: Gold coated, off-axis parabolic mirror used in PTR system to increase the signal to noise ratio of the detector by collecting more IR radiation.

Therefore, for an ideal mirror focusing into the detector should fill the FOV of the detector with minimal excess. Optimizing the mirror collecting the infrared radiation from the sample is not as straight forward. Assuming the mirror diameter is constant, the shorter focal length the more radiation will be collected. Therefore if the size of signal is being optimized, the shortest focal length is ideal. However, with a short focal length of the sample size will decrease the spot size seen by the detector. Depending on what the beam diameter, sample properties, and modulation speed this can be advantageous or detrimental. In this PTR setup several mirrors are used depending on the heating scenario and sample. They are used to either increase the signal to noise ratio or to increase the detection area.

5.5 Lock-In Amplifier

Lock-in amplifiers are a critical component in any frequency domain photothermal technique. In frequency domain photothermal techniques the modulated temperature amplitude can be quite small which leads to a very small signal. Detecting a small signal is difficult, and in PTR systems the modulated signal is often much smaller in amplitude than the noise level. This is the motivation for the lock-in amplifier. It extracts the signal by

filtering all frequencies except for the modulation frequency where it amplifies it. After this process it measures the amplitude and phase of this signal compared to a reference signal. In the case of PTR the reference signal is provided by the signal generator used to modulate the AOM.

Two different lock-in amplifiers were used in this PTR system. They are Stanford Research Systems SR830 & SR844 seen in figure 5.5. The main difference between these two lock-in's are their effective frequency range. The SR844 is capable of operating between 25 kHz and 200 MHz , where the SR830 is capable of operating between 1mHz to 102.4 kHz . Depending on the sample's optical and thermal properties and heating power the effective range in which a frequency scan could be conducted will vary. The experimental data taken in this work is presented in Chapter 7 was taken using the SR844 lock-in amplifier, however, in the setup and calibration both lock-in amplifiers were used with similar results under the overlap frequency range.

5.6 Optic Accessories

There are several necessary optical accessories for a working PTR system. They include mirrors, windows, neutral density filters, lenses, and irises. Mirror are obviously needed to direct the beam and precisely locate it on the sample.

Some detectors have windows built in that only transmit infrared light. Since methods



Fig. 5.5: Image of the lock-in amplifiers used in the PTR system to filter out noise and amplify the detector signal at the modulation frequency.

of obtaining transfer functions wanted to be tested, an external window was chosen so the wavelengths of light entering the detector can be changed. In this design it was determined that a germanium window is optimal.

Neutral density filters are optical elements that attenuate a certain percentage of light by either reflecting or absorbing it. They are termed neutral density because they are supposed to attenuate the light equally regardless of its wavelength. These are necessary in a PTR system depending on the sample. Depending on the sample properties it is possible to significantly increase the temperature of the sample. If the sample is delicate or sensitive to temperature this could be damaging and should be avoided. This can be done by reducing the laser power by introducing a neutral density filter to the optical path.

As previously discussed the size of heating beam is often critical in determining whether a one dimensional heating solution can be used. The laser beam diameter can be adjusted with the use of different focal length lenses.

When the laser beam goes through an AOM, several beams come out the other side. This is due to the multiple diffractions at integer Bragg angles. Typically either the 0th order beam or the 1st order diffracted is used. With either choice it is necessary to block the other beams, and the best way to do this is with a small iris.

Chapter 6

Analytical and Numerical Results

This chapter will discuss the results from the efforts to bring greater understanding to the physics and numerics of PTR measurements. This has been done through the use of analytical and numerical tools. This chapter begins with a discussion of the differences between the two different heating regimes discussed in Chapter 2. Next results from a Monte Carlo Uncertainty analysis will be presented including a sensitivity study for input parameters. Additionally a non-dimensional analysis on the one dimensional solution is given which yields four dimensionless numbers, and aids in the explanation of the sensitivity study.

6.1 Two Dimensional vs One Dimensional Heat Transfer

In any research application it is necessary to have a good understanding of the physics occurring in the experiment. In Chapter 2 the differences in the one dimensional and two dimensional heat transfer were provided. In addition, it was cited that by integrating the surface temperature of a two dimensional heating scenario, the one dimensional signal will be obtained. This can also be proved through the use of a Hankel transform. However, this is non-trivial since it is known the phase and amplitude of the signal are functions of radius and size of the spot.

To confirm these results, and to gain more knowledge about the physics of the heating scenario; Equation 2.13 was numerically evaluated as a function of r . In addition, the temperature was integrated as a function of r beginning at $r=0$. Figure 6.1 shows the amplitude and phase of the complex surface temperature, integrated phase of the complex surface temperature, and the one dimensional heating solution. It can be seen from this figure how the amplitude and phase of the surface temperature changes as a function of

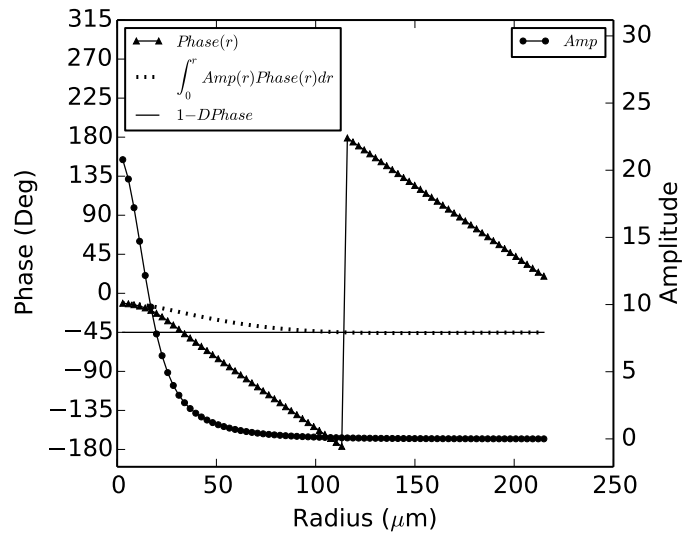


Fig. 6.1: Plot of: the phase of the surface temperature as a function of radius, the $\int_0^r \text{Amp}(r)\text{Phase}(r)dr$, the one dimensional phase, and the amplitude(r). The plot is given for a homogeneous sample of stainless steel with a heating spot radius of $20 \mu\text{m}$.

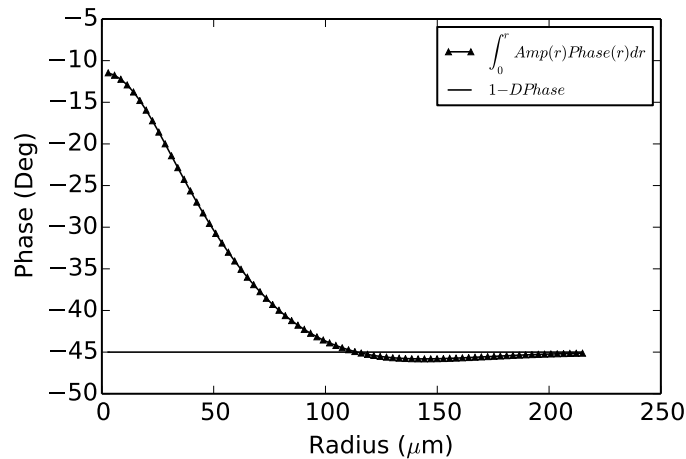


Fig. 6.2: Integrated phase of the surface temperature as a function of radius plotted with the one-dimensional phase at the surface of a homogeneous sample. Plot is given for a homogeneous sample of stainless steel with a heating spot radius of $20 \mu\text{m}$.

distance from the heating spot. The linear relationship of phase as a function of distance outside the heating spot should also be noted. The slope of this line corresponds to the thermal diffusion length determined by the samples diffusivity and modulation frequency of the heating. Figure 6.2 is a subset of Figure 6.1 to help display how the phase "overshoots" the one dimensional result at first, but then converges back to it as the integration continues. This is the phenomena that occurs when the detector integrates the emitted infrared radiation over the surface of the sample.

The phase at the center of the heating spot is determined by the thermal diffusion length and the diameter of the heating laser. If the heating laser is highly focused and the thermal diffusion length is much longer than the heating laser diameter then the phase will begin at 0° at the spot and decay from there. This meaning the temperature of the sample at the center of the heating spot is in phase with the heating laser. As the spot size become larger the phase lag at the center of the spot will increase until it becomes -45° at which the thermal diffusion length is much smaller than the laser heating spot diameter and one dimensional heating has been obtained.

6.2 Non-Dimensional Analysis

A dimensional analysis was performed on the solution given in Equations 2.8-2.12 to reduce the number of parameters and obtain a deeper understanding of the physics involved. The dimensionless parameters found are given in equations 6.1 through 6.4.

$$Fo_j = \frac{k_j}{\omega C_j L_j^2} = \frac{\alpha_j}{\omega L_j^2}, \quad (6.1)$$

$$Bi_j = \frac{L_j h_j}{k_j}, \quad (6.2)$$

$$\pi_1 = \frac{C_1 k_1}{C_2 k_2} \quad (6.3)$$

$$\pi_2 = \frac{Q}{\Theta_o h_1} \quad (6.4)$$

The first parameter given by equation 6.1 is a dimensionless time scale commonly found

in heat transfer known as the Fourier number, and defined by the ratio of thermal wave period to the characteristic heat diffusion time in the materials layer [18]. Equation 6.2 is also a common dimensionless parameter known as the Biot number, which characterizes the ratio of convection heat transfer to conduction heat transfer [18]. Equation 6.3 defines the third dimensionless number which will be referred to as π_1 , which is the ratio of effusivities. This value was found by Almond and Patel [11] to quantify the thermal mismatch at the interface between the two materials, and determines the magnitudes of the reflection and transmission of thermal waves at the interface. The final parameter is the ratio of characteristic surface heat flux to convective heat loss, defined in equation 6.4 as π_2 . Expressing Equations 2.8-2.12 in these parameters, the non-dimensionalized thermal wave field solution becomes equations 6.5 through 6.7.

$$\Theta^* = \frac{\pi_2 Bi_1 \sqrt{Fo_1}}{2\sqrt{2}(1+i)} \left(\frac{(1+R_1)(1+\rho_{21} e^{-\frac{2(i+1)}{\sqrt{2Fo_1}}})}{1 - R_1 \rho_{21} e^{-\frac{2(i+1)}{\sqrt{2Fo_1}}}} \right) \quad (6.5)$$

$$\rho_{21} = \frac{(1 - \sqrt{\frac{1}{\pi_1}}) + R_2(1 + \sqrt{\pi_1}) e^{-\frac{2(1+i)}{\sqrt{2Fo_2}}}}{(1 + \sqrt{\frac{1}{\pi_1}}) + R_2(1 - \sqrt{\pi_1}) e^{-\frac{2(1+i)}{\sqrt{2Fo_2}}}} \quad (6.6)$$

$$R_j = \frac{(1+i) - Bi_j \sqrt{2Fo_j}}{(1+i) + Bi_j \sqrt{2Fo_j}} \quad (6.7)$$

6.3 Sensitivity

In any experiment, it is necessary to understand how each input parameter effects the results, and more specifically how sensitive the results are to variations in the inputs. This section discusses the results of a sensitivity study conducted with input parameters.

Thermal property measurements are conducted using thermal wave techniques by detecting the amplitude and phase of the surface temperature as referenced from the heating laser. These measurements are then conducted for a range of frequencies, which is commonly called a frequency scan. Finally the thermal properties are determined by fitting a theoretical model to the sample response data. However, the fitting process relies on the

accuracy of known parameters. These parameters often include the number of layers in the sample, the thickness of the layers, and some of the thermal properties. A common scenario is when the substrate material is known, and the film thickness is known, but the thermal properties of the film are unknown. In this case the thermal properties of the film will be measured. The accuracy of these properties will be determined by the accuracy of the parameters that are used in the fitting process. A sensitivity study has been conducted to determine which parameters affect the resulting thermal properties the most.

To calculate these sensitivities theoretical frequency scans were simulated with the “correct” value of the input parameters (substrate thermal properties and layer thicknesses). Then the theoretical model was fit with a specified variation of the input parameter. For the example of film thickness, equation 2.8 was used with the correct thickness of the film to obtain a response of Θ . Then when equation 2.8 was fitted to the response of Θ for diffusivity and effusivity a different value was used for the film thickness. This difference between the input value use for the physics simulation and curve fit results in error from the fit.

The results of this sensitivity analysis are displayed in table 6.1 and figure 6.3. The most unique result is the nonlinear relationship between uncertainties of film diffusivity and film thickness shown in figure 6.3. This nonlinear relationship can be explained by Equation 6.1 in the dimensional analysis where ω and L are related nonlinearly. From a closer inspection of these dimensionless parameters it is predicted that all other relationships should be linear if correlated at all. This prediction was confirmed from the sensitivity study conducted, and the results are presented in table 6.1.

Table 6.1: Correlations between input parameters and the fitted film diffusivity and effusivity

Parameter	α Sensitivity	ϵ Sensitivity
Film Thickness	Nonlinear	Uncorrelated
Substrate α	Uncorrelated	Uncorrelated
Substrate ϵ	Uncorrelated	Linear (1:1)
Frequency	Linear (1:1)	Uncorrelated

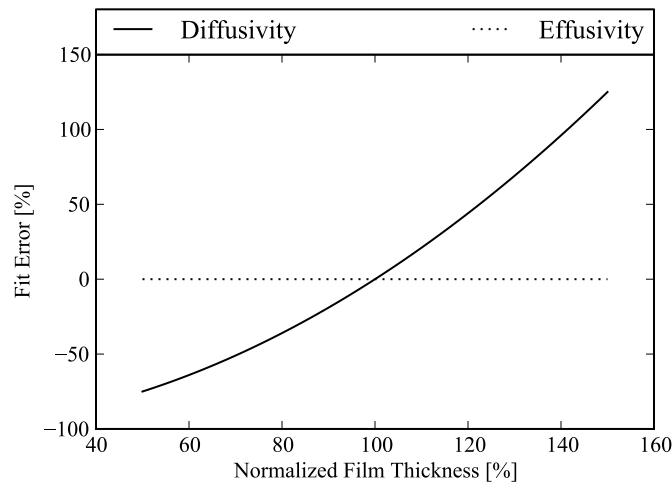


Fig. 6.3: Sensitivity plot of diffusivity and effusivity as the “measured” value for layer thickness is varied in the curve fitting process.

6.4 Log vs Linear Spacing

In front detection, frequency domain, PTR measurements, the phase and amplitude of the surface temperature is measured as a function of frequency. Therefore, it is necessary to determine a set of frequencies at which to measure the sample. The two methods that have been used by researchers are linear or log spacing of sampled frequencies between a initial and final frequency. If data is taken at a large number of sampled frequencies either spacing technique the fitting process will obtain the same result. This comparison was conducted to determine which spacing method will obtain more accurate results from the same number of data points. To test the difference in spacing, frequency scans were generated between an initial and final frequency. The scans were conducted with increasing number of points until there was no difference in the results between the two methods.

It can be seen from figures 6.4 and 6.5 that as the number of samples taken increases the results for linear and logarithmic spacing of the frequencies converge to the same result as expected. However, at low number of samples logarithmic spacing of samples produces significantly better results. With either spacing method the beginning and final frequencies need to be selected such that they capture the frequencies where the layered structure

interference will effect the phase and amplitude of the temperature.

6.5 Monte Carlo Overall Uncertainty

Experimental data often need to be combined to compute the final result through a data reduction process (DRP), which can be based on either an equation or algorithm. In the Monte Carlo method hypothetical parameter uncertainty distributions are generated based on prior knowledge and expected uncertainties. These values can be measured experimentally with instruments or based on instrument/material specifications. The Monte Carlo process uses a randomly selected set of input values to compute the result of the DRP. The statistical properties of the output distribution are then used to describe the uncertainty characteristics of the result. Because the actual input values for each Monte Carlo sample are randomly selected from their parent distributions, their reduction is also random, and belongs to the parent distribution of the computed results. When enough samples are taken, the statistical characteristics of the input and output distributions will converge to stable values, which are the input and output uncertainties, respectively. This process can be very computationally intensive, and for many non-trivial DRP's will require significant computer resources.

The input uncertainties considered in the Monte Carlo Simulation are displayed in Table 6.2. Each of these input parameters and their specific uncertainty distributions were used in the Monte Carlo simulation. The simulation begins with the “correct” values for each of these parameters. Next the substrate thermal properties and film thickness are “measured” (pulling a random value from the parent distribution of the parameter). From

Table 6.2: Table of the Monte Carlo input parameters and their uncertainty.

Input	Uncertainty
Film Thickness	5%
Measured Phase(transfer function)	0.5 °
Measured Phase(lock-in)	1 °
Substrate Diffusivity	4.75%
Substrate Effusivity	3.0%
Frequency Uncertainty	0.0083 Hz

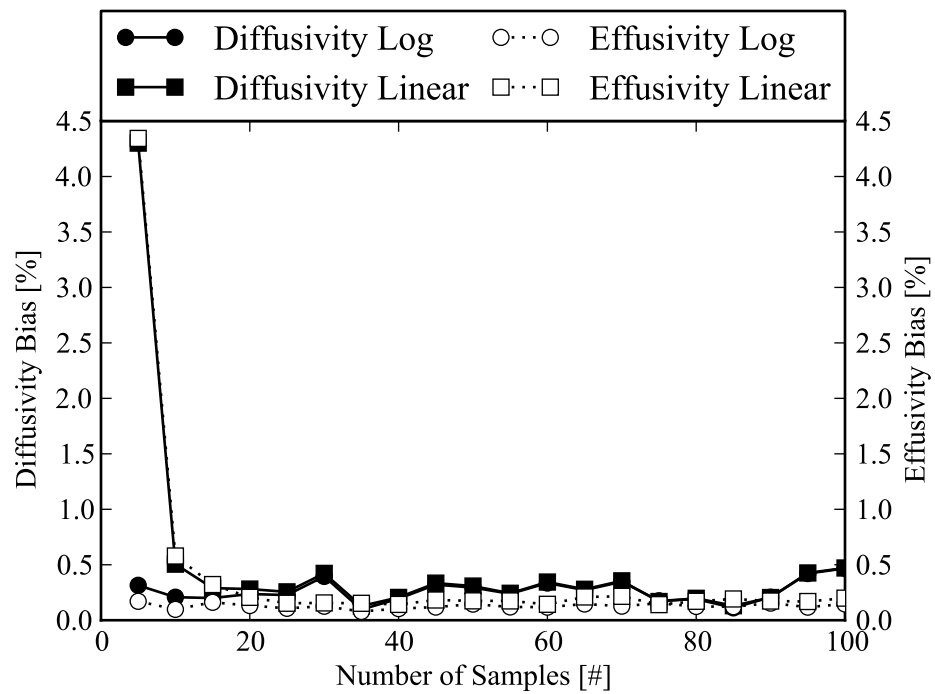


Fig. 6.4: Comparison of logarithmic and linear frequency spacing. Bias uncertainty in effusivity and diffusivity are plotted as a function of the number of frequencies sampled.

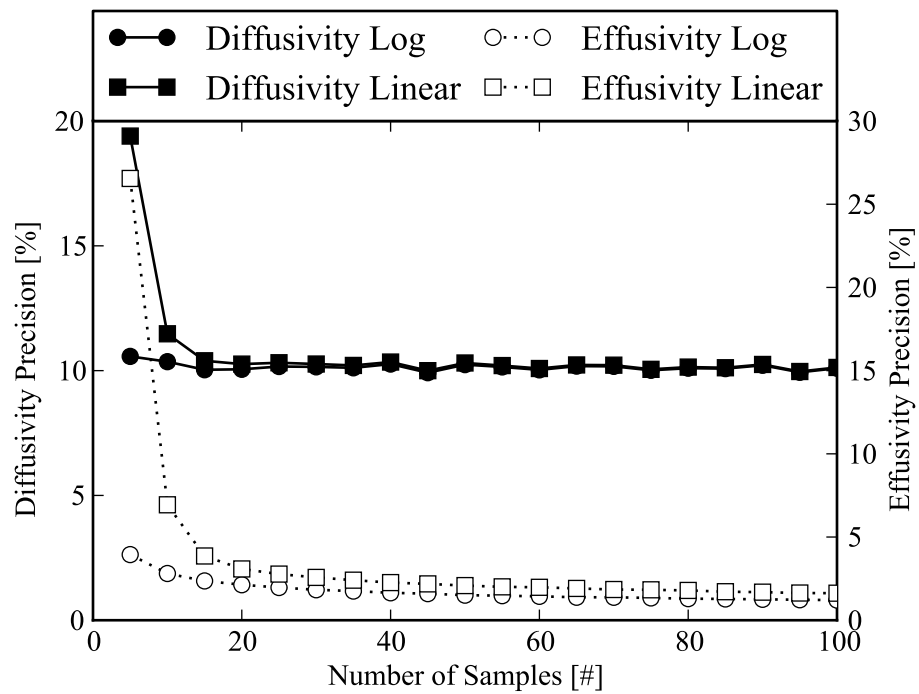


Fig. 6.5: Comparison of logarithmic and linear frequency spacing. Precision uncertainty in effusivity and diffusivity are plotted as a function of the number of frequencies sampled.

here the simulation performs a numerical frequency scan using the "correct" values. After the frequency scan data is generated the phase uncertainty values were added to the frequency scan data. Finally film thermal properties are fitted using the "measured" values for the other parameters. This process is conducted many times, and from these results a distribution for the film thermal properties can be determined. A diagram of the Monte Carlo program can be seen in figure 6.6. The resulting distribution is unique to the input uncertainty distributions used. While in reality many different uncertainty input distributions exist, only one characteristic set was simulated. However, this set of input uncertainty distributions were evaluated for various film and substrate materials to determine how the variations can effect overall uncertainty. From this study it was determined that the uncertainty was dependent on the material, even with the same uncertainty percentage on the thermal properties. The trend displayed the largest uncertainty resulted from the largest mismatch in thermal properties between the substrate and film materials. This result is intuitive since the interaction is dependent on a mismatch between the layer properties at the interface.

The diffusivity bias uncertainty for all combinations were around 0.4% with a precision uncertainty approximately 10.2%. The measurements for effusivity yielded a bias uncertainty of approximately 0.15% and precision uncertainty of approximately 3%. These uncertainties results are specific to the input distributions. The actually uncertainty on a frequency domain PTR measurement will depend significantly on the specific scenario.

Thermal conductivity can be determined from thermal effusivity and diffusivity $k = \epsilon \cdot \sqrt{\alpha}$. By using Taylor's series uncertainty propagation the uncertainty can be computed as $u = \sqrt{u_{\epsilon}^2 + u_{\alpha}^2/4}$.

An important result to note is the output distributions for thermal properties were slightly skewed, and had a small bias. This is due to the nonlinear sensitivity to film thickness. As it can be seen from the sensitivity study, underestimating the film thickness results in less error than overestimating the film thickness by the same amount. The results provided here used a relatively small film uncertainty value, and therefore only resulted in

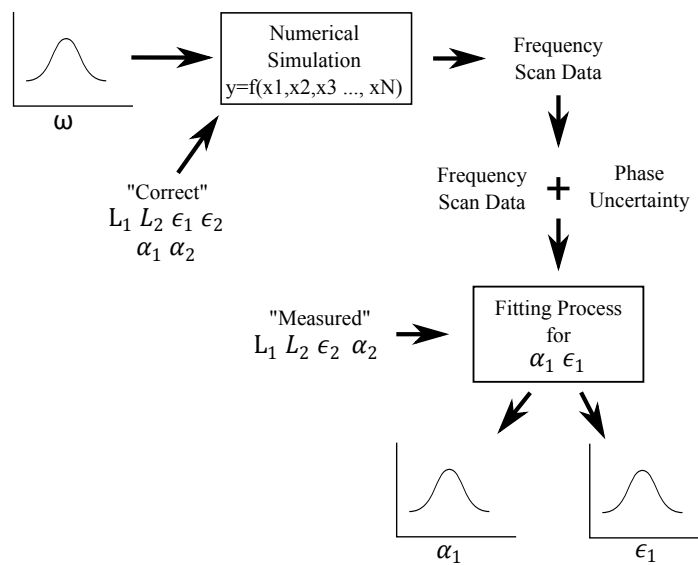


Fig. 6.6: Diagram of the Monte Carlo Simulation applied to PTR.

a small bias and slightly skewed distribution. If a larger uncertainty on film thickness is present a larger bias and skewed distribution should be expected.

Chapter 7

Experimental Methods

For any experimental result, it is as important to understand the method as it is to understand the results and conclusion. For any experiment to be reproducible, a detailed explanation of the experimental setup and procedure is necessary. This chapter will discuss in detail the experimental set up and procedure used in this work. This discussion will begin with the laser modulation procedure, then the alignment of the PTR system, continue with the process used to measure a transfer function, and end with the procedure used to measure samples.

7.1 Laser Modulation

Optimal laser modulation is a necessary component of a PTR system. Frequency domain PTR systems rely on detecting the modulation of temperature due to the modulated heating by a laser. For this reason the techniques used for laser modulation will be discussed in detail.

7.1.1 Laser

As most lasers, the laser used in this work required a “warm up” time before the laser cavity would reach steady state operation. Prior to this steady state operation the pointing direction, laser intensity, and profile vary with time. Therefore, all alignment adjustments and measurements were done after the warm up period of the laser. Furthermore, after warm up it was determined the laser provided the best stability when operating under moderate power conditions. If the sample required low heating power, it is often advantageous to operate the laser under moderate power conditions and use a ND filter to reduce the power of the laser.

7.1.2 Acousto Optical Modulator

An acousto optical modulator (AOM) was used to modulate the laser in this study. As discussed in the literature review, AOMs utilize the interaction between phonons and photons. In AOM's the interaction causes the laser to diffract into multiple beams. The 0th order beam is the one where no diffraction has occurred. The 1st order is the first beam above or below the 0th order beam, and so on. The intensity of these diffracted beams are a function of the angle of incidence of the laser beam to the crystal. Optimal diffraction occurs at a specific angle based on the wavelength of light, called the Bragg angle.

In this work, the AOM is mounted on an angle adjustable mount which is then mounted on a three axis stage. For optimal performance the laser needs to propagate through the center of the crystal, the incident angle needs to be optimized, and the needs to have the correct orientation with respect to the crystal. To attain the optimal performance the AOM was adjusted with the 3-axis stage, changing the position of the laser on the crystal until the maximum modulation amplitude was attained. Next, the incident angle was adjusted likewise, until the maximum modulation amplitude was achieved. These two steps were repeated until the diminishing returns were negligible. The polarization orientation of the light should be noted as AOM crystals have different transmission efficiencies based on the direction of the polarization. The laser used here required a 90 degree rotation of the AOM to match the polarization for optimal performance. The effective bandwidth of AOMs are dependent on the beam diameter, and therefore it can be advantageous to focus a laser beam before entering an AOM. In this research the AOM response was sufficient without focusing the beam and therefore not used.

7.1.3 Wave Form Generator

AOMs require an RF Driver in order to generate the standing phonon waves in the crystal. The RF driver used in this study uses an input from an external wave form generator to determine the intensity of the diffracted beams. For the particular driver and AOM used in this study the optimal input from the wave form generator was a sinusoidal wave with a maximum value of 800 mV and a minimum of 350 mV. This waveform created the largest

modulation amplitude while maintaining the sinusoidal waveform.

7.2 Mirror Alignment

As discussed in Chapter 2, the PTR signal from the detector depends largely on the detection area. The area “seen” by the detector is defined by the size of the detector and the optics used between the sample and the detector. Off-axis parabolic mirrors are often used in PTR systems to control the detection area and increase the infrared radiation received by the detector. The alignment of these mirrors is critical since it plays a large part in determining the detection area and signal strength. Therefore, a detailed description of this alignment process used in this work is included.

7.2.1 1st Mirror and Sample

From practice, it has been determined the easiest configuration to align is when the sample and stage are both on 3-axis stages, and the parabolic mirrors are mounted on optical post rails. Other setups were used in this work, but through the process this setup obtained the best results. Additionally, out of the other methods used, this provides the fastest means to obtain an aligned system.

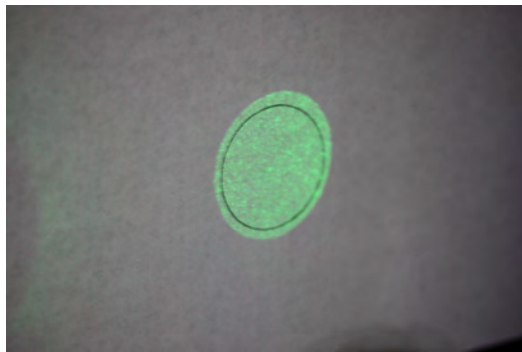
The alignment process begins by first aligning the off-axis parabolic mirror that collects the emitted radiation from the sample. The focal point of this mirror should be on the plane of the samples surface, and located concentric to the heating spot. By definition, all light rays coming from the focal point of mirror will be reflect parallel in the y-direction of the parabola. Therefore, the best way to determine when the mirror is aligned is to have many light rays coming from a point on the surface, and then observe how they are reflected. When this mirror is aligned the reflected light will all be parallel and traveling 90 degree from the vector pointed from the focal point to the mirror. This is due to the fact that the mirrors used in this study of 90 degree off-axis mirrors.

The most practical way to align the first mirror is to mount the sample/target on a three axis stage and mount the parabolic mirror on an optical post mount. Good judgment should be used in getting the alignment close by the use of a tape measure or ruler. Next

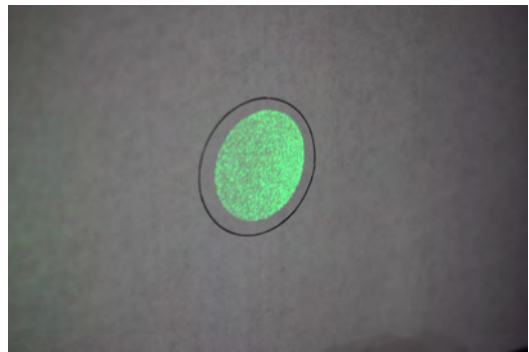
a laser should be focused on the surface by placing a spherical lens in the optical path approximately at the focal length of the lens away from the sample. Since laser light is very close to parallel, this will focus the laser spot into a very small spot size. The objective of the alignment process is to precisely place the focused spot size at the focal point of the mirror. This is done by moving the sample by use of the stage it is mounted on, and by moving the laser by use of adjustable mirrors.

For clarification of the alignment process the direction normal to the optical table will be defined as the y-axis, the direction normal to the sample will be defined as the z-axis, and the direction to the right of the sample, if facing the front, will be defined as the x-axis. The stage will be moved in the z-direction to move the sample into the focal plane. The adjustable mirror the laser is reflected off, will be used to locate where the laser contacts the sample, therefore adjusting the x and y position. Since the laser does not come into the sample normal to the surface, as the sample moves in the z-direction the laser spot's x and y position will also change.

If the sample needs to be adjusted a lot in the z-direction, it may be necessary to reposition the spherical lens that focuses the laser beam since distance from the sample to the lens may no longer be the focal length. To make the alignment process easier, a long focal length spherical lens should be used so that any adjustment lengths are small in comparison to the focal length. Therefore, making the repositioning of the spherical lens



(a) Mirror too close to sample



(b) Mirror too far away from sample

Fig. 7.1: Mirror misalignment in the z-direction.

unlikely. In the alignment process, a "cross hair" target was used, to mark where the focal point of the mirror is once it has been aligned. During the alignment process the location of the cross hairs are not important, only the location of the laser spot. Once optimal alignment has been attained, the x and y directions of the sample stage are adjusted such that the laser spot contacts the intersection of the cross hairs.

There are three types of misalignment in the system corresponding to the three direction of travel of the samples stage. Each of the misalignment types can be determined from observing the reflection from the parabolic mirror. The off-axis parabolic mirrors used in this research have a diameter of 1.5 inches. This diameter is measured on a plane normal to the axis of the parabola where the reflecting surface is projected onto. For example, if the equation of the parabaloid was

$$z = x^2 + y^2, \quad (7.1)$$

the normal plane would be the x-y plane, and if the reflecting surface of the mirror was projected onto this plane it would form a circle with a diameter of 1.5 inches. Therefore, if the parabolic mirror is in good alignment with the laser spot; the reflected rays will make an image of a circle with a diameter of 1.5 inches. Additionally, if the alignment is good, these light rays are parallel, and this image will not change as the light travels further away. For this reason a circle with a diameter matching that of the mirrors was drawn on a piece of paper to be used as an alignment tool. This alignment tool is what is shown in figures 7.1 -7.6 with the reflection of the green laser off the parabolic mirror.

Figure 7.1(a) shows what reflection will occur if the xy position is in good alignment, but the sample is too close to the mirror. It can be seen that the shape of the reflection remains a circle, but it forms an image larger than the mirror size. Additionally, if the alignment tool is moved further away from the mirror the circle will increase in size; further demonstrating the light is not parallel to each other.

In figure 7.1(b) the opposite misalignment is shown, where the sample is too far away from the mirror. Similar to figure 7.1(a), the shape remains a circle, but in this case the size

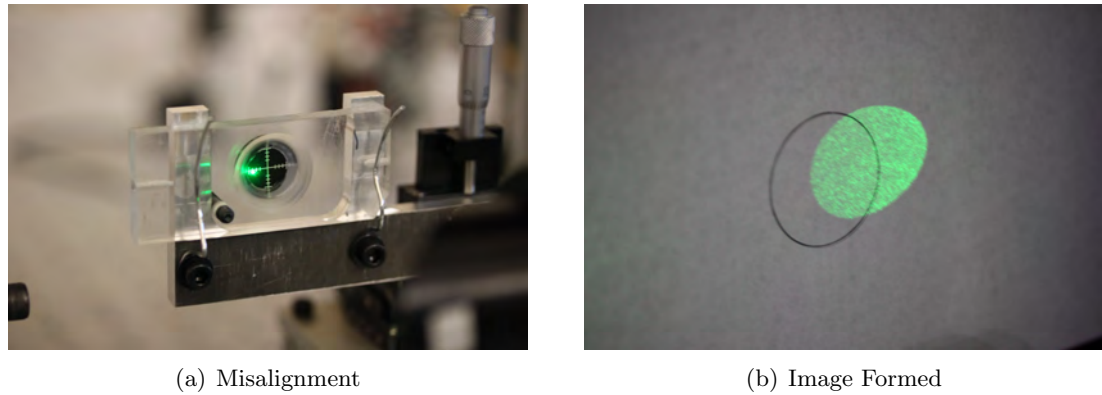


Fig. 7.2: The misalignment and the imaged formed if the laser is to the left of the focal point of the mirror. The target has been placed at the focal point of the mirror.

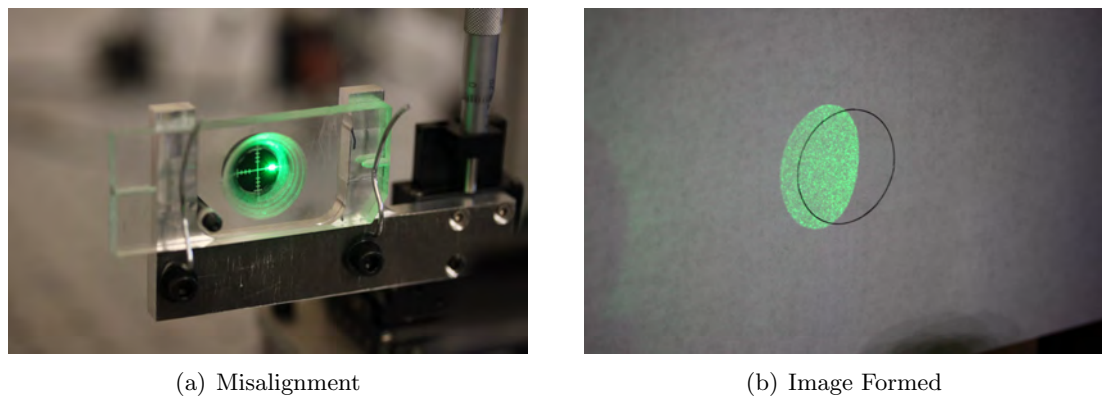


Fig. 7.3: The misalignment and the imaged formed if the laser is to the right of the focal point of the mirror. The target has been placed at the focal point of the mirror.

is smaller than the alignment tool. Similarly if the alignment tool is moved further away the image will continue to decrease in size. However, with this case, if the alignment tool continues to move away the image will eventually become expanding again. This distance will be a function of the mis alignment of the mirror and the focal length.

Next, the alignment in the x-direction will be discussed. As previously discussed, the adjustable mirror that directs the laser is what is used to align the x and y directions. The two misalignments for the x direction are shown in figures 7.2 and 7.3. Unlike misalignment in the z direction, mis alignment in the x-direction produces very different reflected images. However, in this case they are relatively the same size. In figure 7.2(a) the system has been previously aligned, and the cross hairs are located at the focal point of the mirror. In the misalignment shown in 7.2(a) produces the image in figure 7.2(b) approximately 12 inches away from the mirror. It can be seen that the image is offset to the right of the alignment, and is also distorted into an ellipse with the major axis in the x-direction.

Similarly in figure 7.3 the laser is mis-aligned to the right. Likewise, the image is approximately the same size as the well aligned case, but the shape is different. In this scenario the shape of the image is an ellipse with the major axis being in the y-direction.

The final direction of misalignment is in the y-direction; which is shown in figures 7.5 and 7.4. In both these cases the image is approximately the same size as the alignment tool, but is shifted the opposite direction of misalignment and distorted. This misalignment creates an ellipse image, but in this case the direction of major axis of the ellipse is a function of the misalignment.

Finally, the well aligned mirror will produce an image of exactly the alignment tool size and shape. It will be independent of distance from the mirror since the light is parallel. It is best to align the mirror with the alignment tool close to the mirror to get it close, and then move it progressively further away as small corrections are made. As the tool moves further away any error will be exaggerated so it will be easier to see the what adjustments need to be made at further distances. This well aligned condition is shown in figure 7.6. After this well aligned condition is obtained, the sample stage should be moved(only in the

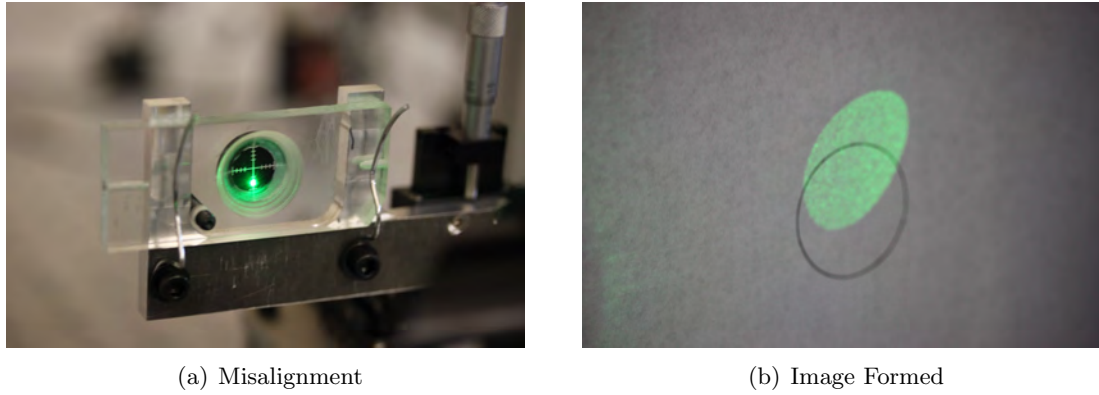


Fig. 7.4: The misalignment and the imaged formed if the laser is below the focal point of the mirror. The target has been placed at the focal point of the mirror.

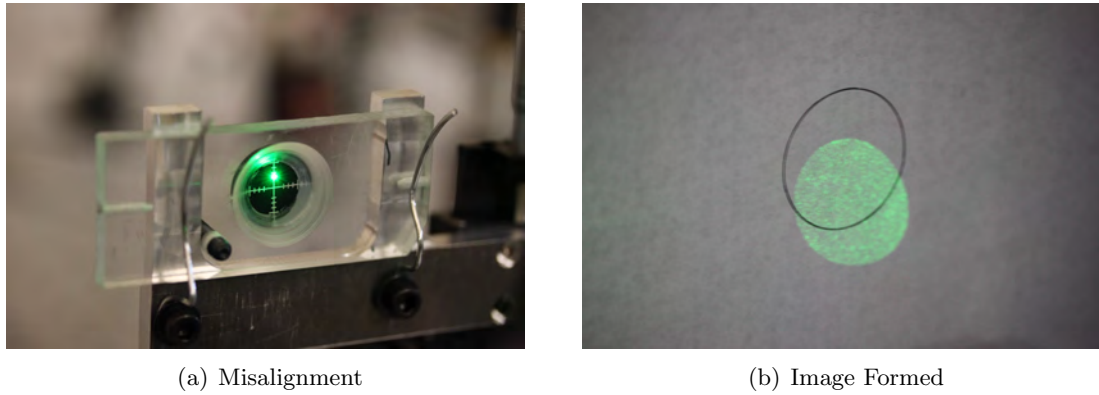


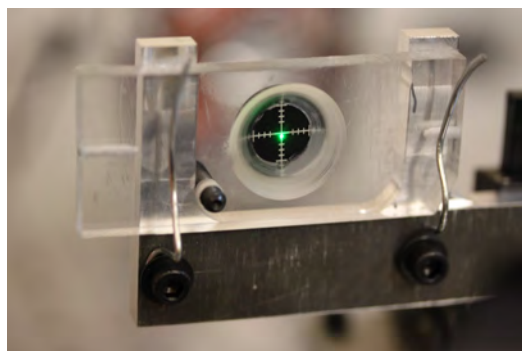
Fig. 7.5: The misalignment and the imaged formed if the laser is above the focal point of the mirror. The target has been placed at the focal point of the mirror.

x and y direction) such that the cross hairs of the target shown are centered in the well aligned laser spot. Therefore the focal spot of the mirror is well defined and is not effected by optical elements that the laser passes through. Therefore optical elements can be added and removed without re-aligning the whole system. The new elements can be added with the target placed as the sample, and then the laser can be adjusted until it is aimed at the target.

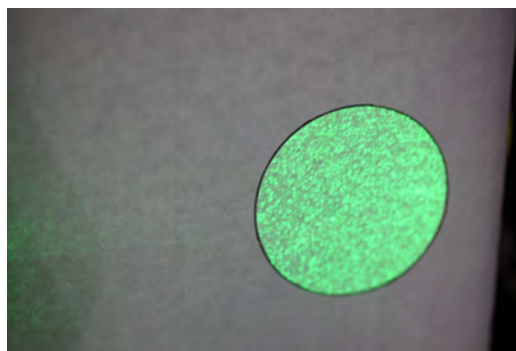
7.2.2 2nd Mirror and Detector

The alignment process of the second mirror is much simpler than the alignment of the first. There are two principles required for it to be aligned. First, the principle axes of the mirror's parabolas need to be aligned with each other. Practically, this is done by placing a straight edge on the back surface of the first mirror and then placing the second mirror such that the back side of the second mirror is also aligned with the straight edge. Second. The elevation of the second mirror needs to match that of the first. This can be done by placing a small level across the two mirrors, or more practically observing the location where all of the light from the first mirror contacts the reflecting surface of the second. Both methods have been used in this study, but the latter is preferred.

The alignment of the detector is the final step in this process. This process is done by illuminating the sample at the focal point of the first mirror, and detecting this in the



(a) Alignment



(b) Image Formed

Fig. 7.6: The well aligned and corresponding image formed.

detector. This is conducted by moving the detector stage in all three directions in a process to optimize for the maximum signal. When this process is being conducted the laser spot should match the same size as the image the detector chip will form on the sample. That is, if the detector chip were illuminating light and it was collected by the parabolic mirrors and focused onto the sample; what would the size of that image be. For example, if the chip size had a 2mm diameter, and the focal length of the parabolic mirrors were the same length, then the image on the sample would be 2mm circle. Therefore in the alignment of this case the laser spot size should be 2mm. This will ensure the maximum will occur at the focal plane of the parabolic mirror. Otherwise it could occur either slightly closer or further away, depending on chip size and heating size. However, if parabolic mirror focal lengths differ, the optical calculations should be done to determine the necessary laser size for proper alignment.

7.2.3 Changing Samples

When testing a new sample, the target should be placed in the sample holder first, and check that the system is still well aligned. After that the sample mounted a sample holder can be mounted on the stage. The sample can then be positioned so the laser is illuminating the location of interest on the sample. Since the position of the laser has been verified to be the focal point of the mirror this is the location that will be observed by the detector. This process makes changing samples very accurate, quick, and simple.

7.3 Calibrating

As discussed in the literature review, the frequency domain PTR measurements measure the temperature's amplitude and phase with respect to the heating laser. This results in the need to calibrate the system to account for the effects that result from the response of the measurement system. In PTR this is done by measuring what is called the transfer function of the system. The transfer function is a set of values where the response of the system has been measured at specific frequencies. Therefore, when a frequency scan is conducted on a sample the measured phase can be adjusted for to remove the response

of the system. In the adjustment process the transfer function phase values are subtracted from the measured phase, and the measured amplitude values are divided by the transfer function amplitude values.

7.3.1 Transfer Function

Originally several methods were attempted to obtain a transfer function. The first was heating a stainless steel or glassy carbon sample and comparing it to the theoretical response. Both of these samples were expected to be homogeneous, and therefore, should obtain the one-dimensional, thermally-thick, solution of -45 degrees. Thereby, any deviation from this -45 would be the measured transfer function. This method was eventually discarded because it relied on the heating a detection being in the one dimensional regime; which was not the case for stainless steel. The other reason for discarding this method was because it relied on the material being homogeneous. While this was probably the case for the stainless steel, the homogeneity of vitreous can be debated depending on the length scale being observed. An additional benefit of using this method is the amplitude of the signal does not decrease with frequency due to the thermal waves magnitude decreasing. Therefore, transfer functions at higher frequencies can be attained with more accuracy.

Given these reasons it was determined that using the MCT detector to detect the heating laser light was optimal. This is possible with our particular PTR setup because the Germanium window regularly used to filter out visible light is external to the detector. Therefore, it can be removed and the detector can observe the laser light. To achieve this the laser was not directly shown into the detector. Instead the scatter light from the samples surface was collected by the parabolic mirrors, and then refocused onto the detector. The power of the laser was turned down very low to begin with to prevent possible damage to the detector, and then was progressively increased until a good signal was obtained.

7.3.2 Calibration Sample

As discussed in the previous subsection, in this work the PTR system measured the laser modulation directly with the IR detector to obtain the response of the system. As

a result of this technique, and the fact that PTR is a direct rather than a comparative measurement technique; this work did not require a calibration sample. However, it is a good validation that the system is working properly and an accurate transfer function has been obtained. Data from the calibration samples will be presented in the Chapter 8.

7.4 Taking Data

In frequency domain PTR, the phase and amplitude of the surface temperature are measured through a range of frequencies. This frequency range is typically centered around a frequency in which corresponds to a thermal diffusion length equal to the thickness of the first layer. The largest interference of thermal waves occurs when this criteria is met. When taking data on the phase and amplitude at these frequencies, there are several parameters the experimenter needs to set. Among the most important include the specifications of the number of frequencies to take data at, the spacing between these frequencies and the number of data points necessary at each location. The number of frequencies and the spacing of the frequencies is investigated numerically in this work. It was determined that the appropriate spacing should be logarithmic, and that 10 frequencies between decades is an appropriate spacing.

7.4.1 Specifying Scan

When measuring a sample properties it is important to consider all of the information known about the sample. Knowledge of the materials structure, how thick the sample is, and if the sample could be layered. As discussed in th literature review, thermal waves reflect and refract at material interfaces.

Additionally, the thermal diffusion length is the parameter that determines how deep the thermal waves will travel into the sample. If the frequency range selected is too high, the thermal diffusion length will be very short an the thermal waves will only penetrate the first layer. This will not yield any useful information about the sample. Likewise, if the frequency range is too low the thermal diffusion length will be long and will not be effected by the top layer. Therefore, for each sample the thermal diffusion length should be

calculated so an appropriate frequency scan can be conducted. If nothing is known about the thermal properties, a large initial range can be scanned to determine what frequencies ranges capture the interference effects of the interface. Next a more refined scan can be conducted around this range.

7.4.2 Lock-in Settings

The lock-in amplifier is one of the most important devices in the PTR system since it is the piece of equipment that measures the phase and amplitude of the detectors signal relative to the heating laser. The lock-in amplifier is essentially a narrow band pass filter centered around the current modulation frequency. Next the lock-in amplifies the signal and compares it to the reference signal. The lock-in then determines the amplitude of the signal and the phase relative to the reference.

Lock-in amplifiers are very useful and versatile, however, their performance is improved when the settings are appropriate for the signal being measured. For the measurements taken in this research a time constant was used of 3 seconds for all measurements. Multiple data points were taken at each frequency for an understanding of the quality of the signal, and the average of these data points were taken as the measurement. In addition to the time constant, the sensitivity is an important setting to note on the lock-in. For this work the sensitivity was set to the smallest value as possible without an overload at the beginning of the scan. Since the amplitude decreases as frequency increases, the sensitivity should be decreased likewise. Since changing the sensitivity changes the integration circuits used, it was changed a few times as possible in a scan. The program controlling the lock-in would change the sensitivity once it sensed it could reduce the sensitivity by an order of magnitude without an overload. This procedure reduces the variables in a frequency scan at an attempt to mitigate errors.

Chapter 8

Measured Results

To understand and quantify the uncertainty and repeatability of PTR measurements it is necessary to measure known samples, and compare the results obtained to those predicted. In addition, it is important to compare the same sample measured using the same method, but with different experimentalists and equipment. The results from these measurements are provided here along with the results from the transfer function analysis. These results were obtained using the experimental setup described in Chapter 5.

8.1 Transfer Function Analysis

As discussed in Chapter 2, the transfer function is used to remove the system response, in phase and amplitude, from the data taken from the sample. In the literature review a few methods for measuring the transfer function were outlined. One method is to detect the laser heating with a photodiode and use that as an input to the lock-in amplifier. Another is to heat a calibration sample such as stainless steel or vitreous carbon and from a theoretical model the sample is predicted, and any deviation from that is said to be the system's response. Lastly IR detectors are most sensitive in the IR wavelength range, but they also detect visible light. The final transfer function method is to detect the laser heating by the same detector used in the measurement.

It has been determined that of these three methods the third method using the IR detector to sense the laser heating directly is the best method to use if allowed by the system. This method is superior to the first method that uses a separate photodiode because it will account for any effect the detector and its preamplifier has on the system. While similar electronics can be used with both detectors, it is ideal to obtain the system response with the system intact. The second method uses all of the same equipment, but relies on

sample homogeneity and a one dimensional heating regime. Obtaining good calibration samples can alleviate the problems of sample homogeneity, but at low frequencies the two dimensional heat transfer will occur and cause the sample's response to deviate from the one dimensional theory. It will therefore be impossible to distinguish this deviation from that of the system.

With the reasoning in this section, this work will use the transfer function obtained using the third method. Depending on the MCT detector this method may not be feasible, since many of them have Germanium windows built in to prevent visible light contacting the detector. If the window is built into the detector this method is not feasible and one of the other two should be used. The transfer function obtained for the PTR system in this work is plotted in figure 8.1.

8.2 Stainless Steel

As part of the validation of the PTR system a homogeneous 304 stainless steel sample was measured in a frequency scan from 10Hz-10kHz. This test was chosen because the material properties are well known, and it is a test of both the detection spot size, and heating spot size because part of the scan is in the two dimensional heat transfer range. Therefore this test confirms the transfer function obtained previously, detection and heating spot size, and the alignment of the system. It can be seen in figure 8.2 the measured data matches very closely to the predicted values. For this measurement a laser spot size had a diameter of 0.5 mm and a detection area of 0.5 mm x 0.5 mm. The numerical simulation used a diameter of 0.5 mm heating laser and a detection diameter of 0.5 mm. The frequency ranges where the one dimensional assumption cannot be made is a difficult region to make a measurement with any certainty because so many parameters are added. However, this is a good test of the system because the sample properties are known and the spot size of the laser is measured and detection area of the sample is calculated. This gives confirmation of these measurements and predictions. Therefore, in the future similar calculations can be made to determine if the one dimensional heating assumption can be made.

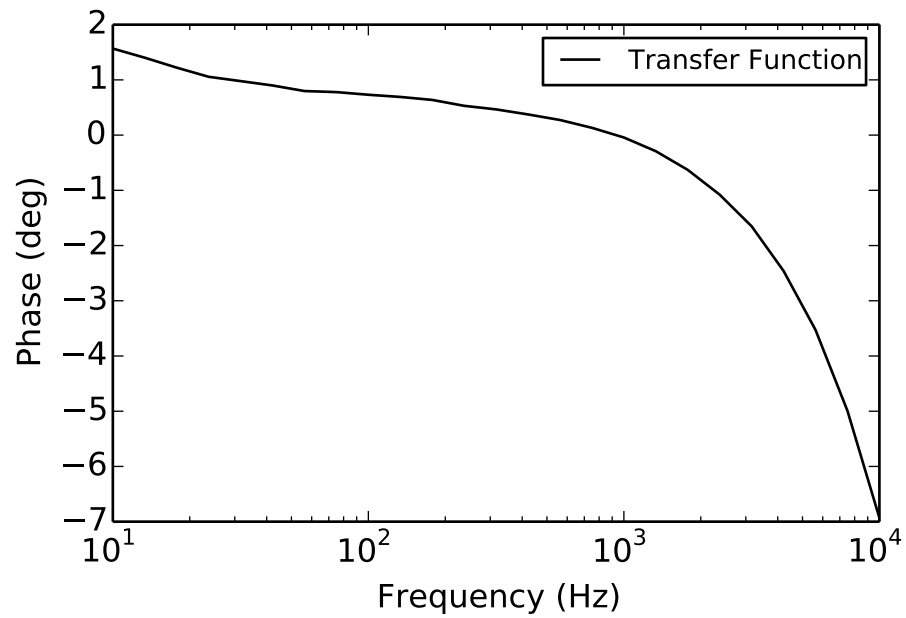


Fig. 8.1: Plot of the transfer function obtained for the PTR system by detecting the laser light directly in the MCT detector.

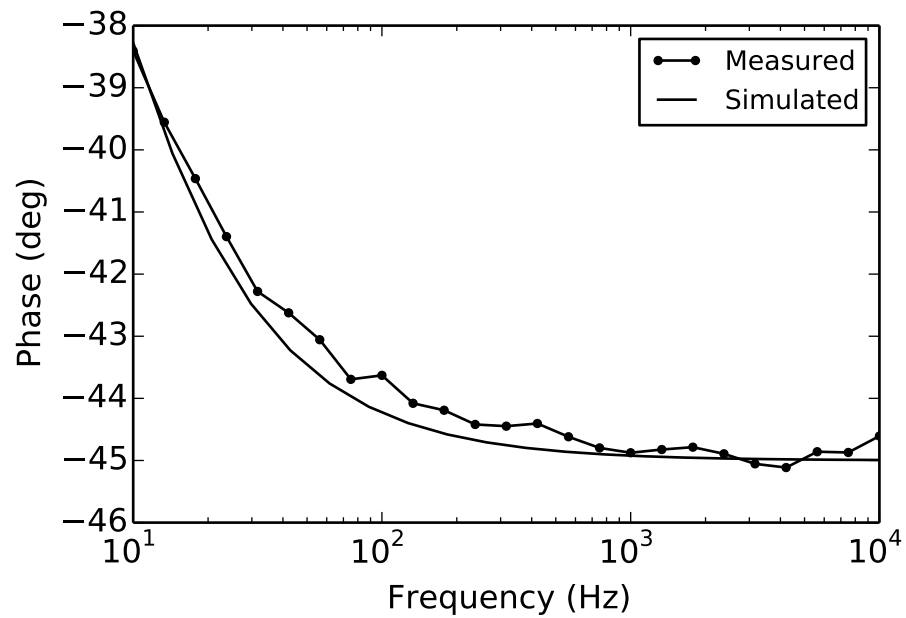


Fig. 8.2: Measured phase and predicted phase of a homogeneous stainless steel 304 sample with detection spot size of 0.5 mm and heating spot size of 0.5 mm.

8.3 ZrC Irradiated Sample

In measurement techniques it is important to understand the uncertainty associated with the measurement, but also the reproducibility. The best measure of reproducibility is when the sample results can be obtained by different experimentalists, with different equipment, using different calibration methods, but applying the same method. That is what was conducted here. A proton irradiated sample of zirconium carbide has been measured independently by Horne and Jensen [6,37] was also measured in this work. The results can be seen in figure 8.3

From these results it can be determined that PTR measurements are repeatable across both PTR systems using different calibration methods and experimental methods. The variation that is displayed in the frequency response could be due to many experimental or sample related factors. Since the experiments took place over the course of several years it is possible/probably the sample changed slightly in the time frame. It is possible the irradiation layer in the sample could have diffused to change the layer thickness, or change the thermal resistance at the interface. Additionally, the sample was fractured to measure the properties on the cross section. This fractured piece is what is measured in this work; Horne's measurements were prior to the fracture. It is possible that damage occurred between the irradiated layers during the fracture which allows for a change in the thermal interface resistance.

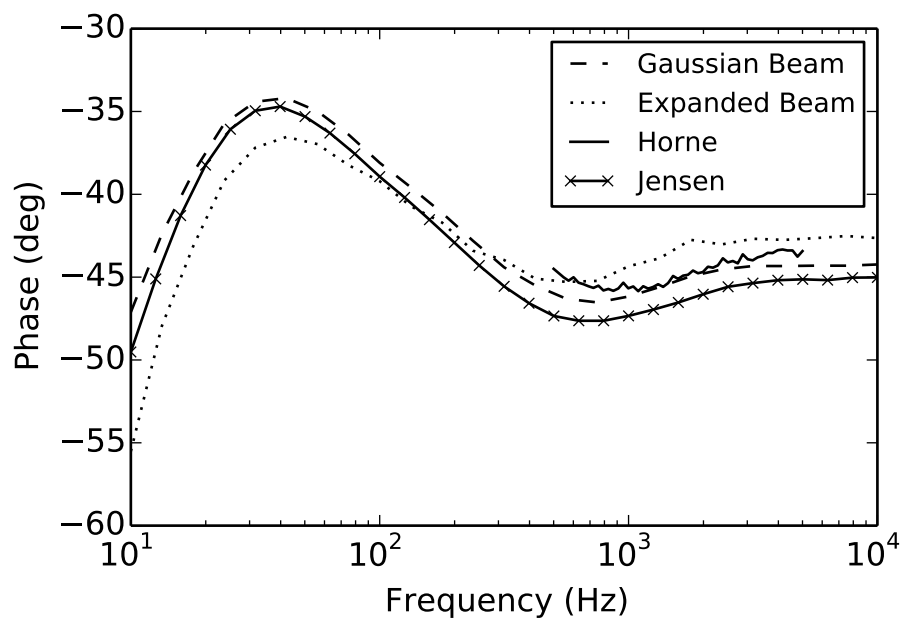


Fig. 8.3: Frequency scan of Proton Irradiated zirconium carbide sample. Plotted along side Horne and Jensen's measurements of the same sample with different PTR systems.

Chapter 9

Conclusions and Summary

Through the course of this work a PTR system was designed, assembled, and calibrated. This system was used to measure an ion irradiated zirconium carbide sample, in addition to calibration samples. The zirconium carbide measurements are compared to two other PTR measurements on the same sample as a repeatability study between PTR systems. Additionally a Monte Carlo method uncertainty analysis was conducted to determine uncertainty in PTR measurements of a coated substrate. Along with this Monte Carlo simulation, a numerical sensitivity analysis was conducted on each of the input parameters. To improve the understanding of the problem, the complex temperature solution to the thermal wave field equation was non-dimensionalized.

The following conclusions can be drawn from this research:

- Four dimensionless parameters governing the two layer thermal wave phenomena have been identified.
- Obtaining a system transfer function by measuring the heating laser directly with the MCT detector is advantageous over other methods for PTR systems with small detector chip sizes without built in germanium windows.
- Logarithmic frequency spacing of data points reduces the uncertainty of PTR measurements.
- In a well-defined two-layered sample, the thermal conductivity of the coating can be measured with 5-6% uncertainty and the thermal diffusivity can be measured with 10% uncertainty.

- Sensitivities of thermal property measurements to input variations have been all been numerically identified as either uncorrelated or linearly(1:1) sensitive with the exception of film thickness.
- PTR can provide repeatable results obtained via different systems and researchers.

References

- [1] Parker, W., Jenkins, R., Butler, C., and Abbott, G., 1961. "Flash method of determining thermal diffusivity, heat capacity, and thermal conductivity," *Journal of Applied Physics*, **32**(9), pp. 1679–1684.
- [2] Gaal, P., Thermitus, M., and Stroe, D., 2004. "Thermal conductivity measurements using the flash method," *Journal of Thermal Analysis and Calorimetry*, **78**(1), pp. 185–189.
- [3] Nunes dos Santos, W., Mummery, P., and Wallwork, A., 2005. "Thermal diffusivity of polymers by the laser flash technique," *Polymer Testing*, **24**(5), pp. 628–634.
- [4] Balageas, D. L., Krapez, J.-C., and Cielo, P., 1986. "Pulsed photothermal modeling of layered materials," *Journal of Applied Physics*, **59**(2), pp. 348–357.
- [5] Tam, A., and Sullivan, B., 1983. "Remote sensing applications of pulsed photothermal radiometry," *Applied Physics Letters*, **43**(4), pp. 333–335.
- [6] Horne, K., Ban, H., Mandelis, A., and Matvienko, A., 2011. "Photothermal radiometry measurement of thermophysical property change of an ion-irradiated sample," *Materials Science and Engineering: B*, **177**(2), pp. 164–167.
- [7] Santos, R., and Miranda, L., 1981. "Theory of the photothermal radiometry with solids," *Journal of Applied Physics*, **52**(6), pp. 4194–4198.
- [8] Mandelis, A., and Chen, Z., 1992. "Lock-in rate-window thermomodulation (thermal wave) and photomodulation spectrometry," *Review of Scientific Instruments*, **63**(5), pp. 2977–2988.
- [9] MacCormack, E., Mandelis, A., Munidasa, M., Farahbakhsh, B., and Sang, H., 1997. "Measurements of the thermal diffusivity of aluminum using frequency-scanned, transient, and rate window photothermal radiometry. Theory and experiment," *International Journal of Thermophysics*, **18**(1), pp. 221–250.
- [10] Salazar, A., R., F., Apinaniz, E., Mendioroz, A., and Celorrio, R., 2011. "Simultaneous measurement of thermal diffusivity and optical absorption coefficient using photothermal radiometry. II multilayered solids," *Journal of Applied Physics*, **110**(3), pp. 033516–033516.
- [11] Almond, D. P., and Patel, P. M., 1996. *Photothermal Science and Techniques*, Chapman & Hall, London.
- [12] Rosencwaig, A., Opsal, J., Smith, W., and Willenborg, D., 1985. "Detection of thermal waves through optical reflectance," *Applied Physics Letters*, **46**(11), pp. 1013–1015.
- [13] Paddock, C., and Eesley, G., 1986. "Transient thermorefectance from thin metal films." *Journal of Applied Physics*, **60**(1), pp. 285–290.

- [14] Li, B., Roger, J., Pottier, L., and Fournier, D., 1999. "Complete thermal characterization of film-on-substrate system by modulated thermoreflectance microscopy and multiparameter fitting," *Journal of Applied Physics*, **86**(9), pp. 5314–5316.
- [15] Hua, Z., Ban, H., Khafizov, M., Schley, R., Kennedy, R., and Hurley, D. H., 2012. "Spatially localized measurement of thermal conductivity using a hybrid photothermal technique," *Journal of Applied Physics*, **111**(10), pp. 103505–103505.
- [16] Rosencwaig, A., and Gersho, A., 1976. "Theory of the photoacoustic effect with solids," *Journal of Applied Physics*, **47**(1), pp. 64–69.
- [17] Erik Nordal, S. and O. Kanstad, 1979. "Photothermal radiometry," *Physica Scripta*, **20**, pp. 659–662.
- [18] Incropera, DeWitt, Bergman, and Lavine, 2007. *Fundamentals of Heat and Mass Transfer*, Wiley, Jefferson City.
- [19] Chirtoc, M., Gibkes, J., Walther, H., Christ, A., Antoniow, J., Bicanic, D., Bozoki, Z., Szabo, G., Bein, B., Pelzl, J., et al., 2001. "Comparative study of coating thickness determination in packaging composite materials using photothermal radiometry, photoacoustic and photopyroelectric methods," *Analytical Sciences*, **17**, pp. 185–188.
- [20] Elek, F., 1999. "An Investigation of Photothermal Radiometric Thermal Diffusivity Measurements of Thin Steel Samples," PhD thesis, University of Toronto.
- [21] Garcia, J. A., Nicolaidis, L., Park, P., Mandelis, A., and Farahkbahsh, B., 2001. "Photothermal radiometry of thermal sprayed coatings: Novel roughness elimination methodology," *Analytical Sciences*, **17**. Pp. s89-s92
- [22] Salazar, A., S´anchez-Lavega, A., and Fernandez, J., 1989. "Theory of thermal diffusivity determination by the miragetechnique in solids." *Journal of Applied Physics*, **65**(11), pp. 4150–4156.
- [23] Salazar, A., S´anchez-Lavega, A., and Fern´andez, J., 1993. "Thermal diffusivity measurements on solids using collinear mirage detection," *Journal of Applied Physics*, **74**(3), pp. 1539–1547.
- [24] Depriester, M., Hus, P., Delenclos, S., and Sahraoui, A., 2005. "New methodology for thermal parameter measurements in solids using photothermal radiometry," *Review of Scientific Instruments*, **76**(7), pp. 074902–074902.
- [25] Mandelis, A., 2001. *Diffusion-Wave Fields Mathematical Methods and Green Functions*, Springer-Verlag, New York.
- [26] Wang, C., and Mandelis, A., 2007. "Case depth determination in heat-treated industrial steel products using photothermal radiometric interferometric phase minima," *NDT & E International*, **40**(2), pp. 158–167.

- [27] Mar'in, E., 2009. *Basic Principles of Thermal Wave Physics and Related Techniques*, Thermal Wave Physics and Related Photothermal Techniques: Basic Principles and Recent Developments, Transworld Research Network, Kerala, India.
- [28] Busse, G., 1980. "Photothermal transmission probing of a metal," *Infrared Physics*, **20**(6), pp. 419–422.
- [29] Fowles, G., 1989. *Introduction to Modern Optics*, Dover Publications, New York.
- [30] Hecht, J., 1992. *Understanding Lasers: An Entry-level Guide*, Wiley-IEEE Press, Piscataway, New Jersey.
- [31] Kanstad, S. O., and Nordal, P.-E., 1986. "Experimental aspects of photothermal radiometry," *Canadian Journal of Physics*, **64**(9), pp. 1155–1164.
- [32] Beckwith, T., Marangoni, R., and Lienhard, J., 2007. *Mechanical Measurements*, Pearson Prentice Hall, Upper Saddle River, New Jersey.
- [33] Horne, K., Ban, H., Fielding, R., and Kennedy, R., 2012. "Monte Carlo uncertainty estimation for an oscillating-vessel viscosity measurement," *Metrologia*, **49**(4), p. 577.
- [34] Greenland, S., 2002. "Sensitivity analysis, Monte Carlo risk analysis, and bayesian uncertainty assessment," *Risk Analysis*, **21**(4), pp. 579–584.
- [35] Cox, M., and Siebert, B., 2006. "The use of a Monte Carlo method for evaluating uncertainty and expanded uncertainty," *Metrologia*, **43**(4), p. S178.
- [36] Coleman, H., and Steele, W., 2009. *Experimentation, Validation, and Uncertainty Analysis for Engineers*, Wiley, Hoboken, NJ.
- [37] Jensen, C., Chirtoc, M., Horny, N., Antoniow, J., Pron, H., and Ban, H., 2013. "Thermal conductivity profile determination in proton-irradiated zrc by spatial and frequency scanning thermal wave methods," *Journal of Applied Physics*, **114**(13), p. 133509.